A regulatory program for initiation of Wnt signaling during posterior regeneration

Alyson N. Ramirez[1], Kaitlyn Loubet-Senear[1] and Mansi Srivastava[2*]

1. Department of Molecular and Cellular Biology, Harvard University, Cambridge 02138, MA, USA
2. Department of Organismic and Evolutionary Biology, Museum of Comparative Zoology, Harvard University, Cambridge 02138, MA, USA

*Corresponding author and Lead contact. Email: mansi@oeb.harvard.edu

Summary

Whole-body regeneration relies on the re-establishment of body axes for patterning of tissue. Wnt signaling is utilized to correctly regenerate tissues along the primary axis in many animals. However, the causal mechanisms that first launch Wnt signaling during regeneration are poorly characterized. We use the acoel worm *Hofstenia miamia* to identify processes that initiate Wnt signaling during posterior regeneration and find that the ligand *wnt-3* is upregulated early in posterior-facing wounds. Functional studies reveal that *wnt-3* is required for regenerating posterior tissues. *wnt-3* is expressed in stem cells, is needed for their proliferation, and its function is stem cell dependent. Chromatin accessibility data reveal *wnt-3* activation requires input from the general wound response. Additionally, the expression of a different Wnt ligand, *wnt-1*, prior to amputation is required for wound-induced activation of *wnt-3*. Our study establishes a gene regulatory network for initiating Wnt signaling in posterior tissues in a bilaterian.

Keywords

Regeneration, axial polarity, acoel, Wnt signaling, wound response, posterior identity

Introduction

Animals capable of whole-body regeneration can replace any missing cell type and re-establish entire body axes. Axial repatterning enables regenerated tissues to acquire correct identities according to their locations in the body plan of the animal. In bilaterians, *i.e.*, animals with distinct anterior-posterior and dorsal-ventral axes, transverse amputation creates two fragments: a “head” fragment with a posterior-facing wound site that must regenerate tail tissue, and a “tail”

fragment with an anterior-facing wound site that must regenerate head tissue. Wound sites generated by a single amputation therefore must initiate and establish distinct anterior and posterior regeneration programs, despite having similar positional identities prior to amputation.

Mechanistic studies of whole-body regeneration in planarians and acoels, two distantly-related bilaterian species (Figure 1A), identified a requirement for Wnt signaling in posterior regeneration (Gurley, Rink and Sanchez Alvarado, 2008; Iglesias *et al.*, 2008; Petersen and Reddien, 2008, 2009; Srivastava *et al.*, 2014). Wnt ligands are highly expressed in posterior tissues in the planarian *Schmidtea mediterranea* and in the acoel *Hofstenia miamia.* Inhibition of Wnt signaling during regeneration causes the transformation of posterior tissues to anterior structures in both species, giving rise to double-headed animals with head tissue forming at both anterior- and posterior-facing wound sites. Conversely, overactivation of Wnt signaling via inhibition of Wnt antagonists during regeneration gives rise to double-tailed animals in both species. Thus, Wnt signaling could represent an evolutionarily conserved mechanism for establishing the identity of posterior tissues in regenerating bilaterians. Furthermore, Wnt signaling is sustained specifically at oral-facing wound sites in *Hydra* and is required for correct regeneration of tissues along the oral-aboral axis, the primary body axis in cnidarians (Nakamura *et al.*, 2011; Vogg *et al.*, 2019). Given the phylogenetic position of cnidarians as the sister-lineage to bilaterians (Figure 1A), the shared role of Wnt signaling in patterning the axial identities of tissues during regeneration could be 1) an ancestral trait that is broadly conserved across metazoans, *i.e.*, it is a homologous process, or, 2) convergently-evolved in multiple lineages possibly via co-option of developmental mechanisms, *i.e.*, it is a homoplastic process (Hall, 2007). A robust assessment of these alternative hypotheses for the evolution of Wnt signaling function during regeneration requires an understanding of how Wnt signaling is initiated upon amputation.

In *Hydra*, two distinct phases of Wnt pathway induction in oral-facing wound sites are known – immediate secretion of Wnt3 protein by apoptotic interstitial cells and later, transcriptional upregulation of *Wnt3* mRNA observed in endodermal epithelial cells (Hobmayer *et al.*, 2000; Guder, 2006; Chera *et al.*, 2009; Nakamura *et al.*, 2011). Studies of the *Wnt3* locus showed that a combination of activation via β-catenin/TCF and repression via Sp5 restricts the Wnt signaling center to the oral end of intact animals (Nakamura *et al.*, 2011; Vogg *et al.*, 2019). Although it has been hypothesized that transient suppression of the repressor must occur to enable *Wnt3* activation at oral-facing wound sites (Nakamura *et al.*, 2011), and expression analysis shows a corresponding absence of *Sp5* prior to *Wnt3* activation (Vogg *et al.*, 2019), the

mechanisms leading to transcription of the *Wnt3* locus upon amputation are not known in cnidarians.

It is also unknown which transcriptional programs induce Wnt ligand expression upon wounding in bilaterians. In planarian regeneration, wound-induced ERK activation is needed for expression of Wnt pathway components (Owlarn *et al.*, 2017). Additionally, mechanisms for inhibition of Wnt signaling specifically at anterior-facing wound sites have been identified (Gurley, Rink and Sanchez Alvarado, 2008; Iglesias *et al.*, 2008; Petersen and Reddien, 2008, 2009; Gaviño *et al.*, 2013; Roberts-Galbraith and Newmark, 2013; Tewari *et al.*, 2018). However, the regulatory logic for initiation of Wnt ligand expression is yet to be identified. The control of Wnt signaling during regeneration has not yet been investigated in acoels. Here, we sought to assess the dynamics of Wnt pathway expression during regeneration and to identify mechanisms that drive its activation upon amputation in *Hofstenia*.

Our analysis of the regeneration transcriptome of *Hofstenia* revealed that Wnt ligands and other posterior markers show upregulated expression at posterior-facing wound sites within six hours following amputation. To find candidate genes for the initiation of this expression, we focused on the earliest asymmetries between anterior- and posterior-facing wound sites during regeneration. We found that a Wnt ligand, *wnt-3*, was substantially upregulated at posterior-facing wounds by three hours upon injury and was required for correct patterning and regeneration of posterior tissues. Further, a combination of a generic wound response factor and a pre-existing patterning gradient activates *wnt-3* at posterior-facing wound sites. Specific establishment of Wnt signaling at posterior-facing wound sites is a shared mechanism for determining correct anterior-posterior specification; our work has identified a regulatory program for the initiation of Wnt signaling during posterior regeneration.

Results

Transcriptomic analysis of regenerating animals identified genes induced at either anterior-facing or posterior-facing wound sites

To identify regulators for initiating Wnt signaling, which is localized to posterior tissues, we sought to understand the dynamics of symmetry breaking during regeneration. We reanalyzed a transcriptome profiling dataset and noted that known anterior and posterior markers were significantly upregulated by 12 hours post amputation (hpa), with most posterior markers significantly upregulated by 6 hpa (Supplemental Figure 1A, B; Gehrke *et al.*, 2019). Wound-induced genes identified in *Hofstenia* thus far were found to be upregulated in both anterior- and posterior-facing wound sites. We reasoned that genes involved in initiation of Wnt signaling

would be induced asymmetrically and focused on genes that were significantly upregulated at posterior-facing wound sites but not at anterior-facing wound sites, or vice versa, at 3 hpa relative to the 0 hpa control time point (Figure 1B). Anterior- and posterior-facing wound sites had ten and eight putatively uniquely-induced genes respectively, that were upregulated by 3 hpa (Supplemental Table S1, Supplemental Figure 1C, D). These genes included transcription factors known in other systems to regulate posterior identity (both during development and regeneration; *brachyury*, *sp5*), factors in known signaling pathways (*smoothened*, *hes, wnt-3*), and other transcription factors (*foxa1*) (Singer *et al.*, 1996; Kavka and Green, 1997; Yamaguchi *et al.*, 1999; Arnold *et al.*, 2000; Estella *et al.*, 2003; Thorpe, Weidinger and Moon, 2005; Weidinger *et al.*, 2005; Fujimura *et al.*, 2007; Martin and Kimelman, 2008; Sun *et al.*, 2008; Morley *et al.*, 2009; Augello, Hickey and Knudsen, 2011; Srivastava *et al.*, 2014; Kennedy *et al.*, 2016; Tewari *et al.*, 2019).

To validate our transcriptomic analysis, we assessed the expression of all 18 genes with *in situ* hybridization in intact animals and in regenerating fragments at 0 hpa, 3 hpa, and 6 hpa (Supplemental Figure 2A, B). Of the genes that showed visible expression, a quarter (4/16; 25%) did not show wound-induced activation, whereas half (8/16; 50%) were expressed in both anterior- and posterior-facing wound sites. Four genes (*ptn14*, *brachyury*, *sp5*, and *wnt-3*) were visibly asymmetrically induced between anterior- or posterior-facing wound sites at 6 hpa. Two genes, *sp5* and *wnt-3*, emerged as the only candidates with induction visible by 3 hpa (Figure 1C, D). Both genes were specifically upregulated at posterior-facing wound sites – no *sp5* expression was observed at anterior-facing wounds and *wnt-3* expression at this location was indistinguishable from its pre-amputation expression level visible in the 0 hpa specimens. We therefore focused on studying these two genes to identify mechanisms for Wnt re-establishment in the posterior as they are homologs of known mediators of Wnt signaling (Clevers, 2006). We note that the *wnt-3* gene in *Hofstenia* represents one of seven Wnt ligands encoded in the transcriptome, none of which have specific orthology to Wnt families in other animals, for example, Wnt-3 in *Hofstenia* is not an ortholog of *Hydra* Wnt3 (Srivastava *et al.*, 2014; Gehrke *et al.*, 2019).

We further validated the dynamics of expression of *sp5* and *wnt-3* during regeneration via quantitative PCR (qPCR) and by extending the time course of expression analysis via *in situ* hybridization (Supplemental Figure 2C-F). Whereas some upregulation (not statistically significant) of *wnt-3* expression in anterior-facing wounds was detected by 3 hpa in transcriptome data (Figure 1C), no visible or significant upregulation of *wnt-3* or *sp5* was found via *in situ* hybridization and qPCR, respectively, in anterior-facing wounds. Both genes were

activated in posterior-facing wound sites by 3 hpa and maintained their expression in the posterior as head fragments continued to regenerate. Further, posterior expression of *sp5* and *wnt-3* was maintained in a gradient in tail fragments, consistent with their known expression in the posterior of intact worms (Srivastava *et al.*, 2014; Tewari *et al.*, 2019). Therefore, we next asked if *wnt-3* and *sp5* play a role in determining the axial identity of tissue during regeneration in *Hofstenia*.

wnt-3 RNAi animals failed to regenerate and showed defects in axial polarity

To assess the role of *wnt-3* and *sp5* during regeneration, we used RNA interference (RNAi) to inhibit gene expression prior to transverse amputation and assessed the capacity of RNAi fragments to regenerate by 8 days post amputation (dpa), when head and tail tissues are by and large restored. We predicted that if *sp5* or *wnt-3* were required for the re-establishment of axial identity during regeneration, polarity defects would be present following RNAi. *sp5* RNAi fragments inconsistently led to defects with anterior (11/58; 18.9%) and posterior (21/56; 37.5%) regeneration (Supplemental Figure 3A). In addition, expression of an anterior and a posterior marker was not affected following *sp5* knockdown at 8 dpa (Supplemental Figure 3B). Notably, RNAi of *wnt-3* led to striking and highly penetrant regeneration deficient phenotypes: head fragments failed to form posterior tissues (135/142; 95%), whereas tail fragments failed to regenerate a visible blastema or mouth (136/139; 97.8%) by 8 dpa (Figure 2A, Supplemental Figure 3C, D). We therefore focused on further characterizing the *wnt-3* RNAi phenotype.

To determine if attenuation of *wnt-3* during regeneration resulted in defects in polarity, we assessed the expression of anterior and posterior markers in *wnt-3* RNAi fragments. *wnt-3* RNAi head fragments expressed anterior markers (*sFRP-1*, *foxD*, and *fz-7*) within posterior-facing wound sites, and failed to express the posterior marker *fz-1,* indicating a mis-specification of the posterior-facing wound site (Figure 2B,C). *wnt-3* RNAi tail fragments showed some expression of the anterior markers *sFRP-1* and *foxD* at the anterior-facing wound site, but relative to control RNAi, the levels of expression appeared reduced (Figure 2B). The expression domain of *fz-7* at anterior-facing wound sites in *wnt-3* RNAi was expanded compared to control RNAi tails, indicating that *wnt-3* is required for restricting expression of anterior markers (Figure 2D). Taken together, the *wnt-3* RNAi phenotype suggests RNAi fragments both (1) failed to correctly specify a new posterior and (2) correctly specified the anterior, but failed to achieve full anterior regeneration by 8 dpa.

The misexpression of anterior markers at posterior-facing wound sites following *wnt-3* RNAi resembled the RNAi phenotype of a previously-studied Wnt ligand, *wnt-1* (Srivastava *et*

al., 2014). However, there are notable differences between regenerating *wnt-3* and *wnt-1* RNAi animals. First, *wnt-1* RNAi tail fragments made a full blastema and a visible mouth by 8 dpa (Supplemental Figure 3E), which *wnt-3* RNAi tail fragments failed to achieve (Figure 2A). Second, although both *wnt-3* and *wnt-1* RNAi head fragments expressed anterior markers ectopically within posterior-facing wound sites, *wnt-1* fragments formed a complete ectopic head with a clear mouth, as assessed by expression of *sFRP-1* (Supplemental Figure 3F). In contrast, *wnt-3* RNAi head fragments expressed *sFRP-1* in posterior-facing wound sites, but these cells did not form coherent structures (Figure 2B). Third, in anterior-facing wound sites, *wnt-1* RNAi tail fragments had no discernible expansion of the *fz-7* expression domain (Supplemental Figure 3G). Conversely, following *wnt-3* RNAi, expression of *fz-7* is expanded in anterior-facing wound sites (Figure 2B, D). Fourth, the expression of *wnt-1* and *wnt-3* during regeneration is distinct. Although *wnt-1* did not emerge as an early posterior wound-induced gene in our transcriptome analysis, it did show an upward trend in expression in posterior wound sites (Figure 2E, Supplemental Figure 3H). However, this was not validated in our experimental studies as we did not detect wound-induced expression of *wnt-1* during regeneration by *in situ* hybridization or by qPCR (Figure 2F, 2G, Supplemental Figure 3I). In contrast, the earliest expression of *wnt-3* in posterior-facing wound sites is wound-induced, and is detectable by 3 hpa in all three measurements (Figure 1D, 2E, 2G, Supplemental Figure 2E, F). Taken together, these results suggest distinct roles for *wnt-3* and *wnt-1* during regeneration.

wnt-3 expression and function involves stem cells

wnt-3 RNAi animals failed to make both anterior and posterior outgrowths. We sought to determine if this phenotype was the result of a general defect in cell proliferation in *wnt-3* RNAi animals, and if a lack of proliferation could underlie the defects we found following *wnt-3* RNAi. In *Hofstenia*, similar to planarians, the only proliferative cells are the neoblasts, a population of effectively pluripotent stem cells that are required for regeneration (Reddien *et al.*, 2005; Srivastava *et al.*, 2014). Phospho-histone H3 immunostaining previously revealed dynamic changes in neoblast proliferation during regeneration in *Hofstenia*. Therefore, we utilized this assay to assess the number of mitotic cells in *wnt-3* RNAi fragments (n > 4 fragments/time point). We detected a decrease in the number of proliferating cells in both head and tail fragments specifically close to the wound site at 72 hpa (Figure 3A, Supplemental Figure 4A, B). This indicates the expression of *wnt-3* is required for cell proliferation within regenerating fragments.

The impact of *wnt-3* RNAi on proliferation in head fragments could be due to the absence of its wound-induced activation in posterior-facing wounds. However, the effect on proliferation in tail fragments could be due to the pre-existing expression of this gene, which forms a gradient with highest expression in the posterior. The decreased number of mitotic figures at wound sites by 72 hpa could be a result of a requirement for *wnt-3* ligands for stem cell proliferation or the migration of these cells to the wound site. Whereas the observed impact on cell proliferation explains the inability of *wnt-3* RNAi animals to make outgrowths, it does not explain the inability of these animals to correctly pattern posterior-facing wound sites.

After finding a striking reduction in cell proliferation following *wnt-3* RNAi, we sought to determine a mechanism for *wnt-3* action during regeneration by asking which tissue types expressed *wnt-3* in intact and regenerating animals. To assess if *wnt-3* was expressed in stem cells, we quantified the co-expression of *wnt-3* with a known neoblast marker (*piwi-1*). Because *wnt-3* is known to be expressed in *Hofstenia* muscle (Raz *et al.*, 2017), we also assessed co-expression of *wnt-3* and a muscle marker (*tropomyosin*), and a tissue with no previously known Wnt expression (neural; *gad-1*) in intact and 6 hpa regenerating head and tail fragments by *in situ* hybridization. *wnt-3* was expressed in all three cell populations we assessed, in both intact and regenerating animals (Figure 3B, Supplemental Figure 4C, D). Notably, significantly more *wnt-3*$^{+}$ cells also expressed *piwi-1* in posterior-facing wound sites at 6 hpa compared to a similar region within intact animals (Welch two-sample *t*-test; *p*-value, 0.0045; Figure 3C; Supplemental Figure 4C; Supplemental Table S4). As *wnt-3* is highly upregulated at 6 hpa within posterior-facing wound sites, the increased proportion of *wnt-3*$^{+}$*/piwi-1*$^{+}$ cells suggests *wnt-3* is wound-induced in the *piwi-1*$^{+}$ population.

Given *wnt-3* is expressed within *piwi-1*$^{+}$ stem cells and *wnt-3* RNAi reduced stem cell proliferation, we next asked if the misexpression of anterior markers following *wnt-3* RNAi, *i.e.*, ectopic *fz-7* expression in posterior-facing wound sites, relied upon stem cells. We irradiated intact *Hofstenia* to ablate the stem cell population and assessed the expression of *fz-7* within regenerating *wnt-3* RNAi fragments. An effect on expression of *fz-7* in the posterior-facing wound site of *wnt-3* RNAi animals would imply that new cell formation or signaling from stem cells within the regenerating fragment contribute to this phenotype. Irradiated worms were injected with dsRNA to inhibit *wnt-3* at 5 days post irradiation (dpi) for three consecutive days and were assessed for expression of the anterior marker *fz-7* at 3 dpa/10dpi (Figure 3D). The posterior-facing wound site expression of *fz-7* in *wnt-3* RNAi heads was lost following irradiation, indicating that stem cells contribute to the *wnt-3* RNAi phenotype (Figure 3D, Supplemental Figure 4E) either through their progeny or via an unknown signaling mechanism. Interestingly,

the anterior expression of *fz-7* within head fragments was expanded following *wnt-3* RNAi (Figure 3E), implying *fz-7* expression can also be reshaped in head fragments following *wnt-3* RNAi without stem cell contribution. Taken together, these observations suggest both stem cells and pre-existing cells contribute to the ectopic expression pattern of the anterior marker *fz-7* within *wnt-3* RNAi fragments. We suggest it is likely that *fz-7* expression is restricted to an anterior domain in wild type and control RNAi animals, whereas *wnt-3* RNAi interferes with this process, implicating a role for *wnt-3* in morphallaxis.

Input from the generic wound response is required for wnt-3 expression at posterior-facing wound sites

Once we established that *wnt-3* is upregulated asymmetrically soon after amputation and that it is required for correct establishment of posterior identity during regeneration, we sought to determine the mechanism for *wnt-3* activation during regeneration. To identify candidate regulators of *wnt-3* expression, we reanalyzed published ATAC-seq data from regenerating fragments (Figure 4A; Gehrke *et al.*, 2019). Using this dataset, we examined the *wnt-3* locus for differentially accessible regions within the promoter and +/- 5kb (10kb total) around the gene locus, and looked for binding sites for known transcription factors contained within these regions. In both anterior- and posterior-facing wound site datasets, we found a region in the promoter of the *wnt-3* locus that shows a significant increase (adjusted *p*-value, 7.79×10^{-5}, anterior-facing dataset; adjusted *p*-value, 3.1×10^{-8}, posterior-facing dataset; Wald test) in accessibility at 6 hpa compared to 0 hpa (Figure 4B, Supplemental Figure 5A). We noted the presence of two binding sites for the general wound response factor Egr within this region. Accessibility of this region is significantly reduced in anterior-facing wound data (adjusted *p*-value, 0.005; Wald test) following *egr* RNAi relative to control RNAi, implying *wnt-3* is transcriptionally regulated by Egr during regeneration (Figure 4B). Because *egr* is upregulated in both anterior- and posterior-facing wound sites (Gehrke *et al.*, 2019), we hypothesized that *egr* is required for wound-induced activation of *wnt-3* in posterior-facing wounds, and performed *egr* RNAi to assess expression of *wnt-3* during regeneration. The wound-induced activation of *wnt-3* at posterior-facing wound sites was diminished relative to controls by 3 hpa, and was completely lost by 5 dpa (Figure 4C). Notably, pre-existing *wnt-3* expression in tail fragments was also lost by 5 dpa. This suggests that *wnt-3* is transcriptionally regulated by an early wound response factor both for wound-induced expression and for maintenance of expression during regeneration. Furthermore, the locus of *wnt-1*, the other Wnt ligand with a known role in mediating regeneration polarity, did not show a dynamic region of chromatin under the control of

egr, which is consistent with the absence of detectable wound-induced activation of *wnt-1* at early time points in regeneration (Supplemental Figure 5B, C). We therefore propose that *wnt-3*, and not *wnt-1*, relays the decision-making that enables *Hofstenia* to begin regenerating posterior tissues at posterior-facing wound sites.

Pre-existing patterning information is required for wnt-3 expression at posterior-facing wound sites

Because *egr* is upregulated at both anterior- and posterior-facing wound sites (Gehrke *et al.*, 2019) and the dynamics of chromatin containing EGR sites in the *wnt-3* locus are similar at both wound sites, the control of *wnt-3* by *egr* does not explain the asymmetric, early wound-induced expression of *wnt-3*. Other factors must feed into this locus either to specifically upregulate *wnt-3* at posterior-facing wound sites, or to downregulate *wnt-3* at anterior-facing wound sites. To assess a potential source of information that results in asymmetric *wnt-3* induction as early as 3 hpa, we asked if pre-existing gradients of Wnt pathway members with known effects on regeneration polarity could play a role in establishing this asymmetry.

We first asked if *wnt-1* was required for asymmetric upregulation of *wnt-3* expression in posterior-facing wound sites. To assess this, we profiled *wnt-3* expression during regeneration using *in situ* hybridization in *wnt-1* RNAi fragments. Following *wnt-1* RNAi, we did not observe wound-induced *wnt-3* induction at posterior-facing wound sites (Figure 5A, Supplemental Figure 6A). In contrast, *wnt-3* RNAi did not affect *wnt-1* expression from 0 hpa to 15 hpa (Figure 5B, Supplemental Figure 6B). Yet, *wnt-1* expression in posterior-facing wound sites was lost by 5 dpa following *wnt-3* RNAi, suggesting that *wnt-3* is required for the maintenance of *wnt-1* at later stages of regeneration (Figure 5B). We hypothesize that *wnt-1* and *wnt-3* regulate each other's expression, albeit in different processes: *wnt-1* is needed for activation of *wnt-3* in posterior-facing wound sites and *wnt-3* is needed for subsequent maintenance of *wnt-1* in regenerating posterior tissue. Notably, we found TCF/LEF sites in open chromatin in the genomic regions surrounding both *wnt-3* and *wnt-1*, which could serve as the loci for this reciprocal regulation (Supplemental Figure 6C, D).

Although *wnt-1* is expressed in amputated head fragments, this expression corresponds to the levels of *wnt-1* mRNA present in this region of the worm prior to amputation. Because *wnt-1* was not detected as wound-induced by 3 hpa via *in situ* hybridization or qPCR, we reasoned that the pre-existing expression of *wnt-1* is responsible for activation of *wnt-3* in posterior-facing wound sites at 3 hpa (Figure 2E, Supplemental Figure 2E, F). This result adds to growing evidence for the role of pre-existing gene expression in regeneration – body-wide

mRNA gradients of genes present prior to injury, including a Wnt ligand (*wntP-2*), have been proposed as an important aspect of the mechanism for robust patterning control during regeneration in planarians (Lander and Petersen, 2016).

Our data showed that *wnt-1* is expressed, albeit not upregulated, at both anterior- and posterior-facing wound sites during regeneration. *wnt-1* could activate *wnt-3* at both anterior- and posterior-facing wounds. Therefore, another factor might act to repress *wnt-3* expression at anterior-facing wound sites, resulting in asymmetric *wnt-3* induction. In planarians, *notum* is required for setting up correct anterior-posterior identity by clearing Wnt expression from anterior-facing wound sites (Petersen and Reddien, 2011; Roberts-Galbraith and Newmark, 2013). While *notum* expression in *Hofstenia* does not appear to be wound-induced or even expressed in the anterior in intact worms, *notum* RNAi results in two-tailed animals (Supplemental 6E, F; Srivastava et al, 2014). Thus, we assessed whether the pre-existing expression of *notum* prior to amputation has a role in suppressing *wnt-3* induction at anterior-facing wound sites. Control and *notum* RNAi animals were indistinguishable with regards to *wnt-3* expression at early time points upon amputation in both head and tail fragments (Supplemental Figure 6G, H). However, *notum* RNAi tails had robust *wnt-3* expression in anterior-facing wound sites with distinct ectopic tail morphology 5 dpa. This was in contrast with control RNAi tail fragments, which had no *wnt-3* expression at the anterior-facing wound site 5 dpa (Supplemental Figure 6G). We propose that whereas *notum* does not regulate wound-induced *wnt-3* activation, it could act more generally by dampening Wnt signals within both head and tail regenerating fragments. While our work has established that *notum* is not required for clearing wound-induced *wnt-3* expression from anterior-facing wound sites, it is plausible that other Wnt regulators or inhibitors could be involved in this process, which could be mediated via transcriptional control of the *wnt-3* locus or post-transcriptional regulation of the transcript or protein.

Our results suggest a model in which a general wound response factor and pre-existing expression of a Wnt ligand are required for the establishment of asymmetric, wound-induced *wnt-3* expression in posterior-facing wound sites by 3 hpa in acoels (Figure 5C). At later time points during regeneration, after the posterior identity decision has been made, *wnt-3* maintains expression of posterior regulators in posterior-facing wound sites in a stem cell dependent manner and restricts the expression of anterior genes.

Discussion

Our investigation of the mechanism for Wnt pathway activation in the posterior in *Hofstenia* revealed the Wnt ligand *wnt-3* was specifically upregulated at posterior-facing wound sites by 3 hpa and was required for correct patterning of posterior tissues. In addition to showing that *wnt-3* function is stem cell-mediated, we inferred a gene regulatory network for the activation of this Wnt ligand in posterior-facing wound sites. Notably, we demonstrate a link between the general early wound response and the initiation of patterning information, showing *wnt-3* is transcriptionally regulated by Egr, an early wound response factor. Given that *egr* is upregulated at both anterior- and posterior-facing wound sites, another input into the *wnt-3* locus is needed to cause the significant expression differences between anterior- and posterior-facing wound sites by 3 hpa. We propose that this input is likely controlled by the pre-existing gradient of another Wnt ligand, *wnt-1*, prior to amputation. The role for *wnt-3* is distinct from that of *wnt-1*, which is needed for posterior regeneration but is not the initiator of the posterior regeneration program.

Wnt signaling centers are re-established in a polarized manner along the primary axis during whole-body regeneration in *Hydra* (cnidarian), *Schmidtea* (planarian), and *Hofstenia* (acoel) (Gurley, Rink and Sanchez Alvarado, 2008; Petersen and Reddien, 2008, 2009; Chera *et al.*, 2009; Nakamura *et al.*, 2011; Srivastava *et al.*, 2014; Gufler *et al.*, 2018; Vogg *et al.*, 2019). Our study of Wnt pathway re-establishment in *Hofstenia* enables cross-species comparisons of this process (Figure 5C).

First, perturbation of wound-induced Wnt ligands affects cell proliferation in both *Hofstenia* and *Hydra* (Chera *et al.*, 2009). Additionally, the control of *wnt-3* in *Hofstenia* by another Wnt ligand (*wnt-1*) bears similarity to the known regulation of the *Hydra Wnt3* locus via *β-catenin/TCF (Gufler et al., 2018)*. However, the identity of the Wnt ligand mediating control via *β-catenin/TCF* is unknown in *Hydra*. In contrast, wound-induced expression of the planarian Wnt ligand *wnt1* is *β-catenin*-independent (Petersen and Reddien, 2009).

Second, the likely direct linkage between a wound response factor and a Wnt locus observed in the *Hofstenia* network (Figure 5) has been hypothesized but not demonstrated in *Hydra*. Control of the *Wnt3* locus in *Hydra* could be through the wound-induced CREB transcription factor, as binding sites are present in this region (Galliot *et al.*, 1995; Kaloulis *et al.*, 2004; Chera, Kaloulis and Galliot, 2007; Nakamura *et al.*, 2011). Based on the phylogenetic positions of cnidarians and acoels, we propose that upregulation of Wnt ligands during regeneration via the combined effect of general wound response factors, Wnt signaling, and the downstream control of cell proliferation could be a general feature of axial regeneration, although the identities of the regulatory factors may differ across species. This hypothesis can

be tested by genetic studies of regeneration in other bilaterians such as planarians. For example, drugs that prevent ERK activation, which normally happens within minutes of amputation in planarians, also inhibit expression of generic wound response transcription factors such as *egr2* and *runt1* and Wnt pathway components such as *wnt1* and *notum* (Owlarn *et al.*, 2017). However, the genetic mediators of ERK signaling and transcriptional control of Wnt pathway gene expression remain to be identified.

Third, the spatial dynamics of Wnt ligand upregulation found in *Hofstenia* differ from those in *Hydra* and planarians. In all three species, wound-induced Wnt ligand expression will be sustained at one end of the primary axis (posterior in acoels and planarians, oral in cnidarians), however, expression at the opposite end, which will not establish a Wnt signaling center, shows differences. In *Hydra*, as well as in the anthozoan cnidarian *Nematostella*, the regenerating aboral end shows some upregulation of Wnt ligands (Lengfeld *et al.*, 2009; Nakamura *et al.*, 2011; Schaffer *et al.*, 2016; Vogg *et al.*, 2019; Wenger *et al.*, 2019); in planarians, substantial upregulation of *wnt1* is observed at anterior wounds (Petersen and Reddien, 2009; Wurtzel *et al.*, 2015). In contrast, we did not detect an appreciable upregulation of *wnt-3* or *wnt-1* at anterior-facing wounds in regenerating *Hofstenia*. Notably, Wnt ligands in *Hofstenia* are expressed in broad gradients with highest expression in the posterior in intact animals, and amputated tail fragments do contain Wnt-expressing cells at anterior-facing wound sites even prior to amputation. Therefore, mechanisms for inhibition of Wnt signaling need to be deployed in the regenerating anterior in acoels, as they are needed in planarians (in the anterior) and cnidarians (at the aboral end). The general wound response factor *follistatin* and the anterior-expressed Wnt antagonist *notum* inhibit Wnt signaling in planarians, ultimately restricting Wnt signaling to posterior-facing wound sites (Gaviño *et al.*, 2013; Roberts-Galbraith and Newmark, 2013). Further studies of transcriptional control of Wnt ligand re-expression in planarians and of Wnt signaling inhibition in cnidarians (in aboral-facing wound sites) and acoels (in anterior-facing wound sites) are needed for more systematic comparisons across the three species.

Fourth, the utilization of Wnts during regeneration in planarians, acoels, and cnidarians possibly occurs in different cell types. Wnt expression has been previously characterized within muscle tissue in acoels and planarians (Witchley *et al.*, 2013; Raz *et al.*, 2017; Scimone, Cote and Reddien, 2017). In planarians, whereas the expression of Wnt ligands required for posterior identity (*wnt1*, *wntP-2*) is highly enriched in muscle tissue (Witchley *et al.*, 2013), signaling centers are established in both anterior and posterior-facing wounds in a stem-cell dependent manner, suggesting a role for stem cells in controlling polarity of regenerating tissues in

planarians (Vásquez-Doorman and Petersen, 2014; Lander and Petersen, 2016; Schad and Petersen, 2020). In cnidarians, Wnt ligands are expressed within both endodermal and ectodermal epithelial cells and Wnt3 protein is activated and secreted by interstitial stem cells upon amputation (Chera *et al.*, 2009; Lengfeld *et al.*, 2009; Nakamura *et al.*, 2011; Petersen *et al.*, 2015; Siebert *et al.*, 2019). However, it is unknown if Wnt signaling from these different cell types serves similar or distinct functions. Here, we demonstrated that *Hofstenia* expresses *wnt-3* within stem, neural, and muscle cells, and that the localization of *wnt-3* is enriched in stem cells during regeneration. Further characterization will be necessary to disentangle the roles of *wnt-3* within each tissue.

Wnt signaling has a well-known role in controlling the primary axis in cnidarians (oral-aboral) and bilaterians (anterior-posterior) during development (Hobmayer *et al.*, 2000; Martin and Kimelman, 2009; Loh, van Amerongen and Nusse, 2016). The shared utilization of the Wnt pathway for axial regeneration, albeit with potentially different initiation programs or cellular mechanisms during regeneration in cnidarians, planarians, and acoels, which diverged 650 million years ago, could reflect two alternative evolutionary histories. First, the use of Wnts in patterning the body axis could have been independently co-opted in each species, potentially redeployed from their role in axial polarity establishment during development (a convergently-evolved, homoplastic process). Second, the differences in the mechanism initiating axial polarity could be indicative of developmental systems drift. In this scenario, the roles of Wnts in patterning body axes during regeneration could have been shared by the last common ancestor (an evolutionarily-conserved, homologous process), and over time the mechanism to initiate Wnt activity upon amputation could have diverged. Further characterization of the development of each species, the role Wnt signaling plays in this process, and the mechanisms used to re-establish polarity in other animals capable of whole-body regeneration will be required to distinguish between these possibilities.

Acknowledgements

We thank Dr. Andrew R. Gehrke for insights and help in analyzing chromatin accessibility data and Dr. D. Marcela Bolaños for blind-scoring of experiments. M.S. is supported by the Searle Scholars Program, Smith Family Foundation, and the National Science Foundation (Award #1652104). A.N.R. is supported by the HHMI Gilliam Fellowship.

Author Contributions

A.N.R. and M.S. designed the study and wrote the manuscript. K.L-S. performed and analyzed cellular co-expression experiments. A.N.R. conducted all other experiments.

Declaration of Interests

The authors declare no competing interests.

Figure Legends

Figure 1: Transcriptomic analysis of regenerating animals identified genes induced asymmetrically at anterior-facing or posterior-facing wound sites. (A) Phylogenetic tree showing the position of acoels such as *Hofstenia* (red text) as a sister-lineage to all other bilaterians, with regenerative capacity and prior knowledge of Wnt utilization in this process. Dashed line indicates a putative relationship between acoels and echinoderms based on an alternative phylogenetic position of acoels as sister to Ambulacraria, proposed by some studies (Philippe *et al.*, 2007, 2011). Black circle, trait is present in at least one species of the lineage shown. (B) Schematics of worms showing naming convention used in this paper to denote anterior- or posterior-facing wound sites, and depicting identification of asymmetrically-activated, early wound-induced genes using a published transcriptome (Gehrke, et al 2019). (C) Transcript per million (TPM) values of *wnt-3* and *sp5* in anterior- and posterior-facing wound sites. (*p*-values, likelihood ratio test; * = $p < 0.001$; ** = $p < 0.0001$; *** = $p < 0.00001$; ns, not significant). (D) *in situ* hybridization expression patterns for *wnt-3* and *sp5* at various hours post amputation (hpa): 0 hpa (control), 3 hpa, 6 hpa, and intact worms. *wnt-3* and *sp5* were expressed specifically at posterior-facing wound sites during regeneration (arrowheads). Scale bars, 100μm.

Figure 2: *wnt-3* RNAi animals failed to regenerate and showed defects in axial polarity. (A) Control and *wnt-3* RNAi fragments at 8 days post amputation (dpa). *wnt-3* RNAi head fragments fail to make new posterior structures (arrow), and tail fragments fail to form an unpigmented blastema (arrowhead). (B, C) Expression of anterior (B; *sFRP-1, foxD, fz-7*) and posterior (C; *fz-1*) markers in control and *wnt-3* RNAi head and tail fragments. Proportions of animals with phenotype in the lower left corner. Scale bars, 100μm. (B) *sFRP-1* was expressed in posterior-facing wound sites of *wnt-3* RNAi head fragments (yellow arrow, shown magnified in inset) and was either diminished in anterior-facing wound sites of tail fragments (20/40; yellow arrowhead) or completely lost (20/40; data not shown). *foxD* expression was detected at

posterior-facing wound sites of *wnt-3* RNAi head fragments (red arrowhead, shown magnified in inset). *fz-7* was expressed in posterior-facing wound sites of *wnt-3* RNAi head fragments (green arrow). In *wnt-3* RNAi tail fragments, *fz-7* was expanded towards the posterior (green arrowhead). (C) Expression of *fz-1* was lost in posterior-facing wound sites of *wnt-3* RNAi head fragments (white arrowhead). (D) Quantification of the expansion of *fz-7* in *wnt-3* RNAi tail fragments compared to control. (n = 20 fragments/RNAi condition; *p*-value < 0.00001, Welch two-sample *t*-test; data are represented as mean ∓ SEM). (E) Expression of *wnt-3* and *wnt-1* in posterior-facing wounds during regeneration in RNA-seq data. (*p*-values, likelihood ratio test; * = $p < 0.001$; ns, not significant). (F) Expression of *wnt-1* by *in situ* hybridization in regenerating fragments from 0 hpa to 15 hpa. There was no visible wound-induced expression pattern of *wnt-1* at any time point during regeneration (ph, pharynx). Scale bars, 100μm. (G) Expression of *wnt-3* and *wnt-1* by qPCR in regenerating posterior-facing wound sites from 0 hpa to 24 hpa. (*p*-values, Welch two-sample *t*-test).

Figure 3: *wnt-3* expression and function involves stem cells. (A) Quantification of phospho-histone H3 ($H3P^+$) foci in head and tail fragments of control and *wnt-3* RNAi animals at 72 hpa. Because $H3P^+$ foci showed regionalized distribution, $H3P^+$ foci per unit area were compared by region (head fragments, 2 regions; tail fragments, 4 regions; n = 10 fragments/RNAi condition; *p*-value, Wilcoxon rank-sum test; ns, not significant; data are represented as mean ∓ SEM). (B) Representative images of cell-type expression patterns for *wnt-3*, assessed by co-expression with tissue markers (*tropomyosin*, muscle; *piwi-1*, stem cells; *gad-1*, neural) in intact worms or 6 hpa regenerating fragments. White arrowheads, examples of co-expressed cells. Scale bar, 10μm. (C) Quantification of cell co-expression at either anterior- or posterior-facing wound sites, and an equivalent site in whole animals (*p*-value, Shapiro-Wilks normality test and Welch two-sample *t*-test; ns, not significant; data are represented as mean ∓ SEM). (D) Schematic of irradiation experiment. Animals were first lethally irradiated, then at five days post irradiation (dpi) were injected with dsRNA for three consecutive days, amputated, and then assessed for expression of *fz-7* at 3 dpa/10 dpi. *wnt-3* RNAi head fragments expressed *fz-7* within posterior-facing wound sites (white arrowhead). Expression of *fz-7* at posterior-facing wound sites in *wnt-3* RNAi heads is lost following irradiation (yellow arrowhead), but the pre-existing domain of *fz-7* expression showed expansion toward the posterior (red arrowhead). Scale bar, 100μm. (E) Quantification of pre-existing *fz-7* expression in irradiated head fragments (n > 10 fragments/condition; *p*-value, Welch two-sample *t*-test; data are represented as mean ∓ SEM).

Figure 4: Input from the generic wound response is required for *wnt-3* expression at posterior-facing wound sites. A) Schematic of ATAC-seq data collection (Gehrke et al, 2019). (B) Schematic of the *wnt-3* genomic locus with ATAC-seq data from anterior-facing wound data mapped. The promoter region contained a regeneration-responsive peak that is variable from 0 hpa (blue) to 6 hpa (magenta) (adjusted *p*-value, $3.1x10^{-8}$, tail dataset; Wald test). This peak contained two EGR binding sites (black lines) and the amplitude of this peak was significantly reduced in *egr* RNAi (green) relative to control RNAi (not shown; adjusted *p*-value, 0.005, Wald test). Control RNAi track has been omitted for clarity. (C) RNAi of *egr* led to loss of wound-induced *wnt-3* expression in regenerating heads (arrowhead) at 3 hpa. By 5 dpa, *wnt-3* expression is lost from both regenerating head and tail fragments in *egr* RNAi animals compared to control RNAi animals. Scale bars, 100μm.

Figure 5: Pre-existing patterning information is required for *wnt-3* expression at posterior-facing wound sites. (A) Expression of *wnt-3* in control and *wnt-1* RNAi regenerating heads. Following *wnt-1* RNAi, *wnt-3* expression was diminished by 3 hpa and failed to be upregulated at the posterior-facing wound site (arrowheads). (B) Expression of *wnt-1* in control and *wnt-3* RNAi heads. RNAi of *wnt-3* did not affect expression of *wnt-1* during the early stages of regeneration prior to 5 dpa, but was required for expression at 5 dpa. ph, constitutive expression in pharynx. Scale bars, 100μm. (C) Models for regulation of Wnt signaling upon amputation in acoels (*Hofstenia*), planarians (*Schmidtea*), and cnidarians (*Hydra*). *Hofstenia* and *Hydra* models depict mechanisms for initiation of Wnt ligand expression in posterior and oral (head) tissues respectively; planarian model depicts mechanisms for Wnt inhibition during anterior regeneration. Legend at top; phylogenetic tree at right depicts evolutionary relationships between the three species. In *Hofstenia*, Wnt ligands are expressed in posterior gradients prior to amputation. Following amputation, Wnt-3 is upregulated in posterior-facing tissues in response to wounding by the transcription factor Egr; this likely direct transcriptional regulation can be verified by binding assays. Wound-induced expression of Wnt-3 also relies on pre-existing expression of Wnt-1. Wound-induced Wnt-3 expression in turn induces expression of other Wnt ligands (Wnt-1), and represses expression of anterior genes (Fz-7) to promote posterior formation. In planarians, the wound-induced factor Follistatin and the Wnt antagonist Notum work to clear Wnts from anterior-facing wound sites, promoting anterior formation. The inputs activating Wnts in planarians are unknown. In *Hydra*, post-translational regulation of Wnt3 protein leads to its secretion by apoptotic cells specifically in oral-facing wound sites

immediately after wounding. Later, *Wnt3* mRNA is transcribed in a β-catenin/TCF-dependent manner and regulated by the head inhibitor Sp5.

STAR Methods

RESOURCE AVAILABILITY

Lead Contact

Further information and requests for resources and reagents should be directed to and will be fulfilled by the Lead Contact, Mansi Srivastava (mansi@oeb.harvard.edu).

Materials Availability

All plasmids and materials generated in this study are available from the Lead Contact.

Data and Code Availability

Original data for RNAseq analysis (Figure 1, 2, Supplemental Figure 1, 3) and ATACseq datasets (Figure 4, Supplemental Figure 5, 6) in the paper are available at DOI: 10.1126/science.aau6173

EXPERIMENTAL MODEL AND SUBJECT DETAILS

Hofstenia miamia animals in this study were taken from a colony derived from an initial population collected in Bermuda (Srivastava et al 2014). Animals within this colony (and all animals used for experiments here) represent a wild-type polymorphic population. Animals were kept in plastic boxes at 21°C in artificial sea water, and fed twice weekly with brine shrimp. These worms produced embryos that hatched; hatchlings were fed twice weekly with rotifers to raise to juvenile animals, which were starved for one week prior to regeneration assays.

METHOD DETAILS

Fixation

Whole animals or regenerating fragments were fixed rocking at room temperature for 1 hour in a 4% paraformaldehyde solution in PBS+0.1% Triton-X-100. Animals were dehydrated gradually into 100% MeOH and stored at -20°C.

Fluorescent in situ hybridization (FISH)

RNA probes for detection of mRNA expression were prepared as previously described (Srivastava *et al.*, 2014; Gehrke *et al.*, 2019). FISH protocol was the same as previously described (Srivastava *et al.*, 2014; Gehrke *et al.*, 2019) with two modifications: 1) All washes were performed with 800uL of solution; 2) Bleach solution was changed to incubation in solution (5% deionized formamide,1.2% H_2O_2, 50% saline-sodium citrate buffer (SSC) in milli-Q water) under a strong light source for 2 hours. Animals were incubated with DAPI, washed briefly, and mounted in Vectashield as previously described in (Srivastava *et al.*, 2014).

Quantitative PCR (qPCR)

Wound sites from amputated fragments were collected (replicates = 3, n = 4 fragments/replicate) at multiple time points during regeneration (0, 3, 6, 9, 15, 24, 48 hpa). RNA was extracted using the Nucleospin RNA XS kit (740902.10, Macherey-Nagel). Extracted RNA was used for cDNA synthesis using the SuperScript III kit (Thermo Fisher 18080044) with random hexamer priming. Expression of target genes was detected using forward and reverse primers (Supplemental Table S3), averaged across replicates and normalized by expression of a housekeeping gene (*gapDH* or *ef1-alpha*) to obtain a ΔCt value. Graphs show averaged relative expression values as $2^{-\Delta Ct}$ with +/- the standard error of the mean. For validation of gene knockdown using qPCR, whole regenerating head or tail fragments were collected at 8 dpa (replicates = 3, n = 3 fragments/replicate).

RNA interference (RNAi)

dsRNA was synthesized and RNAi was performed as previously described in (Srivastava *et al.*, 2014; Gehrke *et al.*, 2019). Animals were soaked in dsRNA resuspended in seawater and injected with dsRNA resuspended in nuclease-free water once a day for three consecutive days. Animals were changed to a fresh dsRNA soaking solution each day following injections (500µL per/well of a 24-well plate, 10-17 worms/well). Animals were either fixed whole, or cut two hours after injection on the last day and allowed to regenerate in fresh seawater for different time points prior to fixation.

Phospho-histone-H3 (H3P) immunostaining

H3P staining on fixed worms was done as described in (Srivastava *et al.*, 2014). Animals were fixed in 2 mL round-bottom tubes and stored in 100% MeOH at -20°C. Animals were bleached overnight in a 6% H_2O_2 solution in MeOH, rocking at room temperature under a strong light

source. The following day, animals were washed three times in 100% MeOH, and gradually rehydrated to PBS+0.1% Triton-X-100. Animals were permeabilized in a Proteinase K solution for 15 minutes (0.1% SDS, 20mg/mL Proteinase K in PBS+0.1% Triton-X) and post-fixed in 4% paraformaldehyde in PBS+0.1% Triton-X-100 for 20 minutes. Animals were washed three times for 10 minutes each in a PBS+ 0.1% Triton-X-100 solution. Permeabilized animals were blocked in 10% Horse serum in PBS+0.5% Triton-X-100 solution for one hour at room temperature, and were then incubated overnight at 4°C with primary antibody (Rabbit anti-H3P antibody, Millipore 06-570) at 1:1,000 concentration. Afterward, animals were washed six times for 10-20 minutes each in PBS+0.5% Triton-X-100. Animals were incubated with secondary antibodies at 1:500 concentration (AlexaFluor488 goat anti-rabbit IgG, Jackson Immunoresearch 111-545-144, resuspended 1:1 in 100% glycerol) in block solution overnight at 4°C. Animals were washed six times for 10-20 minutes each in PBS+0.5% Triton-X-100, incubated with DAPI for 45 minutes and mounted using Vectashield as described previously (Srivastava *et al.*, 2014).

Irradiation experiments

Whole animals were exposed to 10,000 rads using a cesium source (our source is 209 rads/minute; animals were exposed to source for 48 minutes in a petri dish filled with seawater). After five days, animals were injected and soaked in dsRNA as described above, then cut and assessed using the *in situ* protocol as described above. Previous studies (Srivastava *et al.*, 2014) have demonstrated a loss of all cycling cells following lethal irradiation by 7 days post irradiation.

Microscopy and image analysis

All fluorescent images were taken on a Leica SP8 microscope. All images are Maximum Intensity Projections unless otherwise indicated. Light images were taken with a LeicaM80 Stereomicroscope with a DFC7000T color camera. Images were processed using FIJI (Schindelin *et al.*, 2012) and Adobe Photoshop.

QUANTIFICATION AND STATISTICAL ANALYSIS

Statistical analysis

Statistical analyses were conducted in R (R Core Team, 2018). Comparisons between the means of two populations were done using either a Welch two-sample *t*-test or Wilcoxon rank sum test. Figure legends and text contain information for statistical tests used in each

experiment, as well as the definition of n and number of samples used for comparisons. Unless otherwise stated, we used the standardized threshold of $p<0.05$ to determine statistical significance.

Analysis of RNA-seq data

Dataset was collected as described in (Gehrke *et al.*, 2019). Briefly, animals were bisected by cutting at the middle stripe and allowed to regenerate for 0, 3, 6, 12, and 48 hours post amputation (hpa) prior to collection of tissue from the wound site. Anterior- and posterior-facing wound sites were collected separately prior to sequencing. All genes included in this analysis had a minimum transcript per million (TPM) value of 5 at 0 hpa, as values below this could confound the analysis. Genes were identified as wound induced (adjusted *p*-value, < 0.05 at 6 hpa compared to 0 hpa; likelihood ratio test) and filtered for significant induction at 3 hpa compared to 0 hpa (*p*-value < 0.001; likelihood ratio test) within the corresponding head or tail dataset (Supplemental Table S1). We first applied the same adjusted *p*-value thresholds to the head and tail datasets, but this criterion effectively removed all tail genes from our analysis. To ensure that tail genes were included, we loosened the significance thresholds for the tail dataset at 6 hpa (adjusted *p*-value, < 0.5) and 3 hpa (*p*-value < 0.005). Due to the looser criteria for the tail dataset, some genes that were significantly induced in the head dataset appeared in the tail list, which was reflected in their expression in our final analysis (Supplemental Figure 1D) and in their *in situ* hybridization patterns (Supplemental Figure 2) at 6 hpa.

ATAC-seq and ChromVAR analysis

ATAC-seq data were collected, analyzed, mapped, and validated as described in (Gehrke *et al.*, 2019). ChromVAR and PIQ analysis was also used as described in (Gehrke *et al.*, 2019) to identify EGR and TCF/LEF binding sites in the *wnt-3* and *wnt-1* genomic loci. Peakset locations and motif locations are provided in Supplemental Table S5.

Quantification of H3P+ foci

Image processing and numbers of $H3P^+$ cells were counted using the image processing program Fiji (Schindelin *et al.*, 2012). Briefly, confocal image stacks were first z-projected. Images were segmented into equal sections (two regions in head fragments, four regions in tail fragments) using the Grid Tool, and the number of $H3P^+$ cells within each region was manually counted. Cell numbers were normalized by the area of the fragment, which was measured by

drawing a region of interest of each segment, thus providing a measure of the number of mitotic cells per unit area (cells/mm^2).

Cell co-expression quantification

Confocal image stacks of stained animals were imaged using a 63X objective, then individual images within each stack were manually assessed for co-expression of *in situ* labels and counted. Quantification was assessed by first identifying *wnt-3*$^+$ cells, and then determining how many of those cells also co-expressed tissue markers. Images were taken from three representative sections of the animal, across several animals per condition (n > 3). Cells were counted by hand and recorded using the Cell Counter plugin in FIJI.

KEY RESOURCES TABLE

Supplemental Table Legends

Table S1, Related to Figure 1: Genes identified in RNA-seq analysis at 6 hpa (top) and 3 hpa (bottom).

Table S2, Related to Figure 1: Summary of *in situ* hybridization results of all genes assessed and GenBank Accession IDs of genes assessed in this manuscript

Table S3, Related to Figure 2: qPCR primers used for validation of expression during regeneration and validation of RNAi knockdown.

Table S4, Related to Figure 3: Raw counts of cells co-expressing tissue markers and *wnt-3*.

Table S5, Related to Figure 4: Scaffold locations of predicted ATACseq peaks and motifs within the *Hofstenia* genome.

References

Arnold, S. J. *et al.* (2000) 'Brachyury is a target gene of the Wnt/β-catenin signaling pathway', *Mechanisms of development*, 91(1-2), pp. 249–258.

Augello, M. A., Hickey, T. E. and Knudsen, K. E. (2011) 'FOXA1: master of steroid receptor function in cancer', *The EMBO journal*, 30(19), pp. 3885–3894.

Chera, S. *et al.* (2009) 'Apoptotic cells provide an unexpected source of Wnt3 signaling to drive hydra head regeneration', *Developmental cell*, 17(2), pp. 279–289.

Chera, S., Kaloulis, K. and Galliot, B. (2007) 'The cAMP response element binding protein (CREB) as an integrative HUB selector in metazoans: clues from the hydra model system', *Bio Systems*, 87(2-3), pp. 191–203.

Clevers, H. (2006) 'Wnt/β-Catenin Signaling in Development and Disease', *Cell*, 127(3), pp. 469–480.

Estella, C. *et al.* (2003) 'The role of buttonhead and Sp1 in the development of the ventral imaginal discs of Drosophila', *Development* , 130(24), pp. 5929–5941.

Fujimura, N. *et al.* (2007) 'Wnt-mediated down-regulation of Sp1 target genes by a transcriptional repressor Sp5', *The Journal of biological chemistry*, 282(2), pp. 1225–1237.

Galliot, B. *et al.* (1995) 'The cAMP response element binding protein is involved in hydra regeneration', *Development* , 121(4), pp. 1205–1216.

Gaviño, M. A. *et al.* (2013) 'Tissue absence initiates regeneration through Follistatin-mediated inhibition of Activin signaling', *eLife*, 2013(2), pp. 1–13.

Gehrke, A. R. *et al.* (2019) 'Acoel genome reveals the regulatory landscape of whole-body regeneration', *Science*, 363(6432). doi: 10.1126/science.aau6173.

Guder, C. (2006) 'An ancient Wnt-Dickkopf antagonism in Hydra', *Development*, pp. 901–911. doi: 10.1242/dev.02265.

Gufler, S. *et al.* (2018) 'β-Catenin acts in a position-independent regeneration response in the simple eumetazoan Hydra', *Developmental biology*. Elsevier Inc., 433(2), pp. 310–323.

Gurley, K. A., Rink, J. C. and Sanchez Alvarado, A. (2008) 'b-Catenin Defines Head Versus Tail Identity During Planarian Regeneration and Homeostasis', *Science*, 319(January), pp. 323–327.

Hall, B. K. (2007) 'HOMOLOGY AND HOMOPLASY', *Philosophy of Biology*, pp. 429–453. doi: 10.1016/b978-044451543-8/50021-6.

Hobmayer, B. *et al.* (2000) 'WNT signalling molecules act in axis formation in the diploblastic metazoan Hydra', *Nature*. doi: 10.1038/35025063.

Iglesias, M. *et al.* (2008) 'Silencing of Smed-betacatenin1 generates radial-like hypercephalized planarians', *Development* , 135(7), pp. 1215–1221.

Kaloulis, K. *et al.* (2004) 'Reactivation of developmental programs: The cAMP-response element-binding protein pathway is involved in hydra head regeneration', *Proceedings of the National Academy of Sciences*, pp. 2363–2368. doi: 10.1073/pnas.0306512101.

Kavka, A. I. and Green, J. B. A. (1997) 'Tales of tails: Brachyury and the T-box genes', *Biochimica et Biophysica Acta - Reviews on Cancer*, 1333(2), pp. 73–84.

Kennedy, M. W. *et al.* (2016) 'Sp5 and Sp8 recruit β-catenin and Tcf1-Lef1 to select enhancers to activate Wnt target gene transcription', *Proceedings of the National Academy of Sciences of the United States of America*, 113(13), pp. 3545–3550.

Lander, R. and Petersen, C. P. (2016) 'Wnt, Ptk7, and FGFRL expression gradients control trunk positional identity in planarian regeneration', *eLife*, 5(April 2016), pp. 1–19.

Lengfeld, T. *et al.* (2009) 'Multiple Wnts are involved in Hydra organizer formation and regeneration', *Developmental biology*, 330(1), pp. 186–199.

Loh, K. M., van Amerongen, R. and Nusse, R. (2016) 'Generating Cellular Diversity and Spatial Form: Wnt Signaling and the Evolution of Multicellular Animals', *Developmental cell*, 38(6), pp. 643–655.

Martin, B. L. and Kimelman, D. (2008) 'Regulation of Canonical Wnt Signaling by Brachyury Is Essential for Posterior Mesoderm Formation', *Developmental cell*, 15(1), pp. 121–133.

Martin, B. L. and Kimelman, D. (2009) 'Wnt Signaling and the Evolution of Embryonic Posterior Development', *Current biology: CB*, 19(5), pp. 215–219.

Morley, R. H. *et al.* (2009) 'A gene regulatory network directed by zebrafish No tail accounts for its roles in mesoderm formation', *Proceedings of the National Academy of Sciences of the United States of America*, 106(10), pp. 3829–3834.

Nakamura, Y. *et al.* (2011) 'Autoregulatory and repressive inputs localize Hydra Wnt3 to the head organizer', *Proceedings of the National Academy of Sciences of the United States of America*, 108(22), pp. 9137–9142.

Owlarn, S. *et al.* (2017) 'Generic wound signals initiate regeneration in missing-tissue contexts', *Nature communications*. Springer US, 8(1), pp. 1–13.

Petersen, C. P. and Reddien, P. W. (2008) ‘Smed-bcatenin-1 Is Required for Anteroposterior Blastema Polarity in Planarian Regeneration’, *Science*, 319, pp. 327–330.

Petersen, C. P. and Reddien, P. W. (2009) ‘A wound-induced Wnt expression program controls planarian regeneration polarity’, *Proceedings of the National Academy of Sciences of the United States of America*, 106(40), pp. 17061–17066.

Petersen, C. P. and Reddien, P. W. (2011) ‘Polarized notum Activation at Wounds Inhibits Wnt Function to Promote Planarian Head Regeneration’, *Science*, 332(May), pp. 852–855.

Petersen, H. O. *et al.* (2015) ‘A comprehensive transcriptomic and proteomic analysis of hydra head regeneration’, *Molecular biology and evolution*, 32(8), pp. 1928–1947.

Philippe, H. *et al.* (2007) ‘Acoel flatworms are not platyhelminthes: evidence from phylogenomics’, *PloS one*. journals.plos.org, 2(8), p. e717.

Philippe, H. *et al.* (2011) ‘Acoelomorph flatworms are deuterostomes related to Xenoturbella’, *Nature*. nature.com, 470(7333), pp. 255–258.

Raz, A. A. *et al.* (2017) ‘Acoel regeneration mechanisms indicate an ancient role for muscle in regenerative patterning’, *Nature communications*. Springer US, 8(1), pp. 1–8.

R Core Team (2018) ‘R: A Language and Environment for Statistical Computing’. Vienna, Austria: R Foundation for Statistical Computing. Available at: https://www.R-project.org/.

Reddien, P. W. *et al.* (2005) ‘SMEDWI-2 is a PIWI-like protein that regulates planarian stem cells’, *Science*. science.sciencemag.org, 310(5752), pp. 1327–1330.

Roberts-Galbraith, R. H. and Newmark, P. A. (2013) ‘Follistatin antagonizes Activin signaling and acts with Notum to direct planarian head regeneration’, *Proceedings of the National Academy of Sciences of the United States of America*, 110(4), pp. 1363–1368.

Schad, E. G. and Petersen, C. P. (2020) ‘STRIPAK Limits Stem Cell Differentiation of a WNT Signaling Center to Control Planarian Axis Scaling’, *Current biology: CB*. Elsevier Ltd., 30(2), pp. 254–263.e2.

Schaffer, A. A. *et al.* (2016) ‘A transcriptional time-course analysis of oral vs. aboral whole-body regeneration in the Sea anemone Nematostella vectensis’, *BMC genomics*. BMC Genomics, 17(1), pp. 1–22.

780 Schindelin, J. *et al.* (2012) ‘Fiji: an open-source platform for biological-image analysis’, *Nature*
781 *methods*. nature.com, 9(7), pp. 676–682.

782 Scimone, M. L., Cote, L. E. and Reddien, P. W. (2017) ‘Orthogonal muscle fibres have different
783 instructive roles in planarian regeneration’, *Nature*, 551(7682), pp. 623–628.

784 Siebert, S. *et al.* (2019) ‘Stem cell differentiation trajectories in Hydra resolved at single-cell
785 resolution’, *Science*, 365(6451). doi: 10.1126/science.aav9314.

786 Singer, J. B. *et al.* (1996) ‘Drosophila brachyenteron regulates gene activity and morphogenesis
787 in the gut’, *Development* , 122(12), pp. 3707–3718.

788 Srivastava, M. *et al.* (2014) ‘Whole-body acoel regeneration is controlled by Wnt and Bmp-
789 Admp signaling’, *Current biology: CB*. Elsevier Ltd, 24(10), pp. 1107–1113.

790 Sun, X. J. *et al.* (2008) ‘Genome-wide survey and developmental expression mapping of
791 zebrafish SET domain-containing genes’, *PloS one*, 3(1). doi: 10.1371/journal.pone.0001499.

792 Tewari, A. G. *et al.* (2018) ‘Cellular and Molecular Responses Unique to Major Injury Are
793 Dispensable for Planarian Regeneration’, *Cell reports*. doi: 10.1016/j.celrep.2018.11.004.

794 Tewari, A. G. *et al.* (2019) ‘A small set of conserved genes , including sp5 and Hox , are
795 activated by Wnt signaling in the posterior of planarians and acoels’, *PLoS genetics*, pp. 1–31.

796 Thorpe, C. J., Weidinger, G. and Moon, R. T. (2005) ‘Wnt/β-catenin regulation of the Sp1-
797 related transcription factor sp5l promotes tail development in zebrafish’, *Development* , 132(8),
798 pp. 1763–1772.

799 Vásquez-Doorman, C. and Petersen, C. P. (2014) ‘zic-1 Expression in Planarian Neoblasts after
800 Injury Controls Anterior Pole Regeneration’, *PLoS genetics*, 10(7). doi:
801 10.1371/journal.pgen.1004452.

802 Vogg, M. C. *et al.* (2019) ‘An evolutionarily-conserved Wnt3/β-catenin/Sp5 feedback loop
803 restricts head organizer activity in Hydra’, *Nature communications*. Springer US, 10(1), pp. 1–
804 15.

805 Weidinger, G. *et al.* (2005) ‘The Sp1-related transcription factors sp5 and sp5-like act
806 downstream of Wnt/β-catenin signaling in mesoderm and neuroectoderm patterning’, *Current*
807 *biology: CB*, 15(6), pp. 489–500.

Wenger, Y. *et al.* (2019) ‘Generic and context-dependent gene modulations during Hydra whole body regeneration’. doi: 10.1101/587147.

Witchley, J. N. *et al.* (2013) ‘Muscle cells provide instructions for planarian regeneration’, *Cell reports*. The Authors, 4(4), pp. 633–641.

Wurtzel, O. *et al.* (2015) ‘A Generic and Cell-Type-Specific Wound Response Precedes Regeneration in Planarians’, *Developmental cell*. Elsevier Inc., 35(5), pp. 632–645.

Yamaguchi, T. P. *et al.* (1999) ‘T (Brachyury) is a direct target of Wnt3a during paraxial mesoderm specification’, *Genes and Development*, 13(24), pp. 3185–3190.

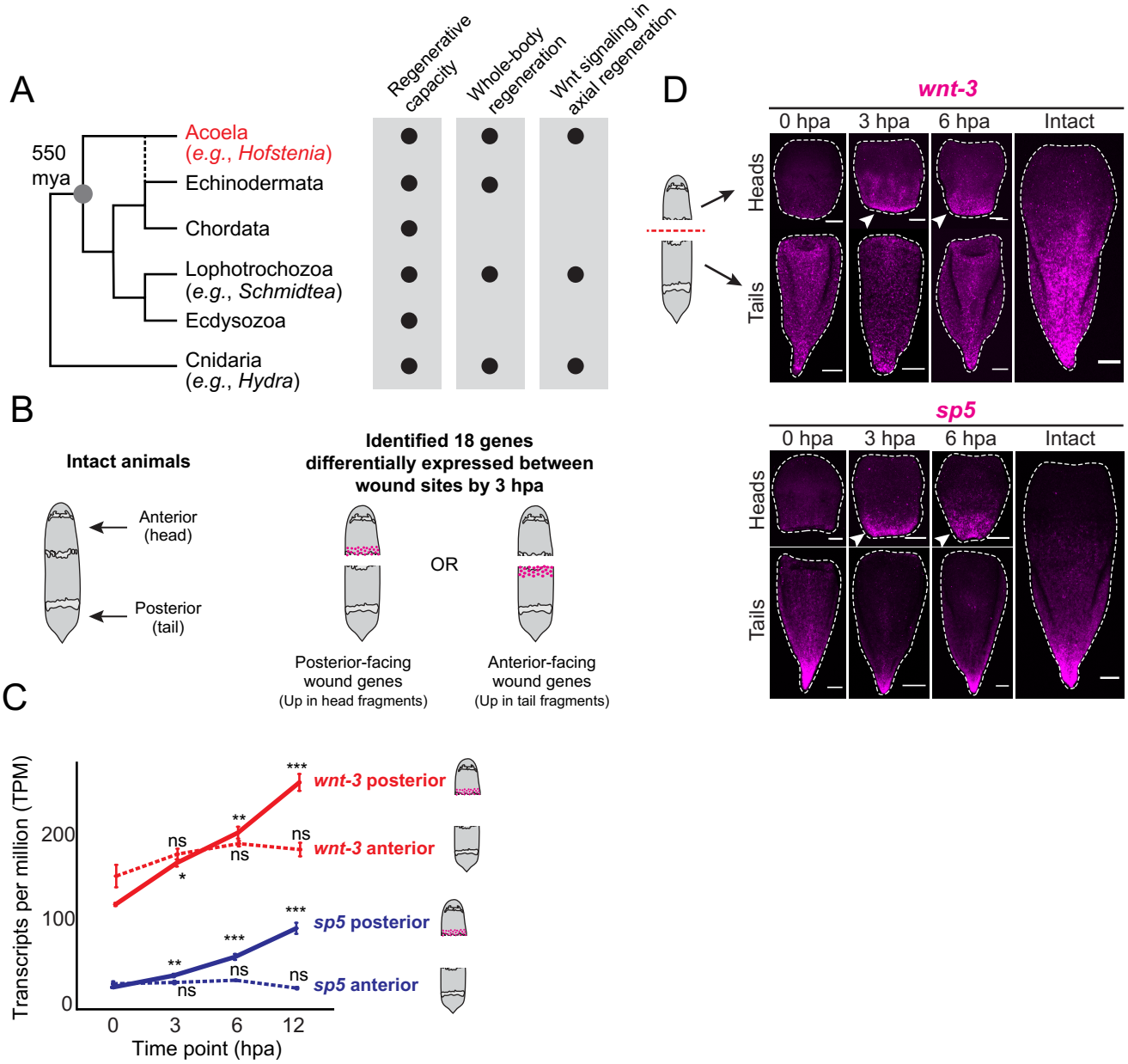
A
550 mya
Acoela (e.g., Hofstenia)
Echinodermata
Chordata
Lophotrochozoa (e.g., Schmidtea)
Ecdysozoa
Cnidaria (e.g., Hydra)
Regenerative capacity
Whole-body regeneration
Wnt signaling in axial regeneration
B
Intact animals
Anterior (head)
Posterior (tail)
Identified 18 genes differentially expressed between wound sites by 3 hpa
OR
Posterior-facing wound genes (Up in head fragments)
Anterior-facing wound genes (Up in tail fragments)
C
Transcripts per million (TPM)
200
100
0
0 3 6 12
Time point (hpa)
wnt-3 posterior
wnt-3 anterior
sp5 posterior
sp5 anterior
***
**
*
ns
D
wnt-3
0 hpa
3 hpa
6 hpa
Intact
Heads
Tails
sp5
0 hpa
3 hpa
6 hpa
Intact
Heads
Tails

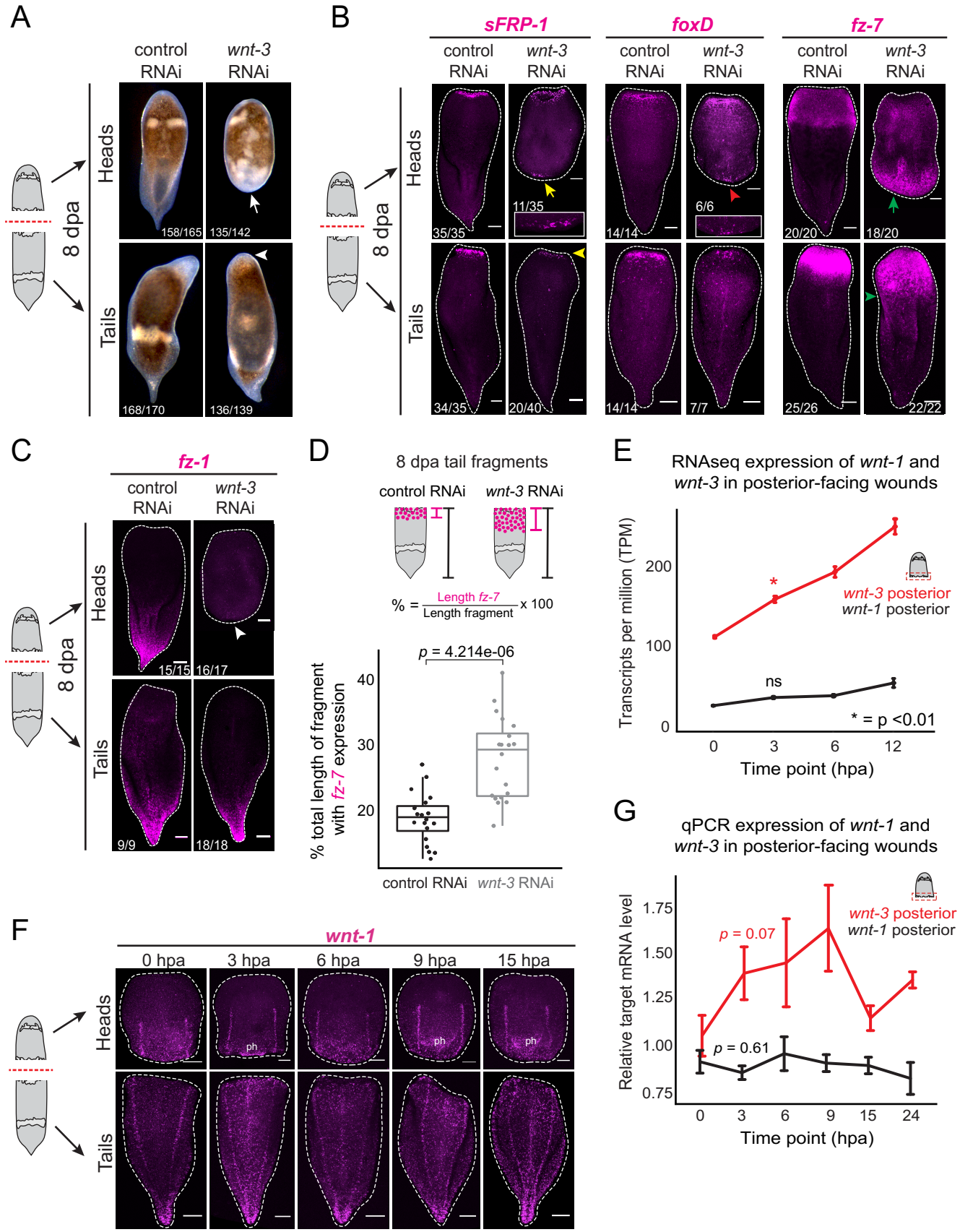
A
control RNAi
wnt-3 RNAi
Heads
Tails
8 dpa
158/165
135/142
168/170
136/139
B
sFRP-1
foxD
fz-7
control RNAi
wnt-3 RNAi
Heads
Tails
8 dpa
35/35
11/35
14/14
6/6
20/20
18/20
34/35
20/40
14/14
7/7
25/26
22/22
C
fz-1
control RNAi
wnt-3 RNAi
Heads
Tails
8 dpa
15/15
16/17
9/9
18/18
D
8 dpa tail fragments
control RNAi
wnt-3 RNAi
% = Length fz-7 / Length fragment x 100
p = 4.214e-06
% total length of fragment with fz-7 expression
40
30
20
control RNAi
wnt-3 RNAi
E
RNAseq expression of wnt-1 and wnt-3 in posterior-facing wounds
Transcripts per million (TPM)
200
100
0
*
wnt-3 posterior
wnt-1 posterior
ns
* = p <0.01
0
3
6
12
Time point (hpa)
F
wnt-1
0 hpa
3 hpa
6 hpa
9 hpa
15 hpa
Heads
Tails
ph
G
qPCR expression of wnt-1 and wnt-3 in posterior-facing wounds
Relative target mRNA level
1.75
1.50
1.25
1.00
0.75
p = 0.07
p = 0.61
wnt-3 posterior
wnt-1 posterior
0
3
6
9
15
24
Time point (hpa)

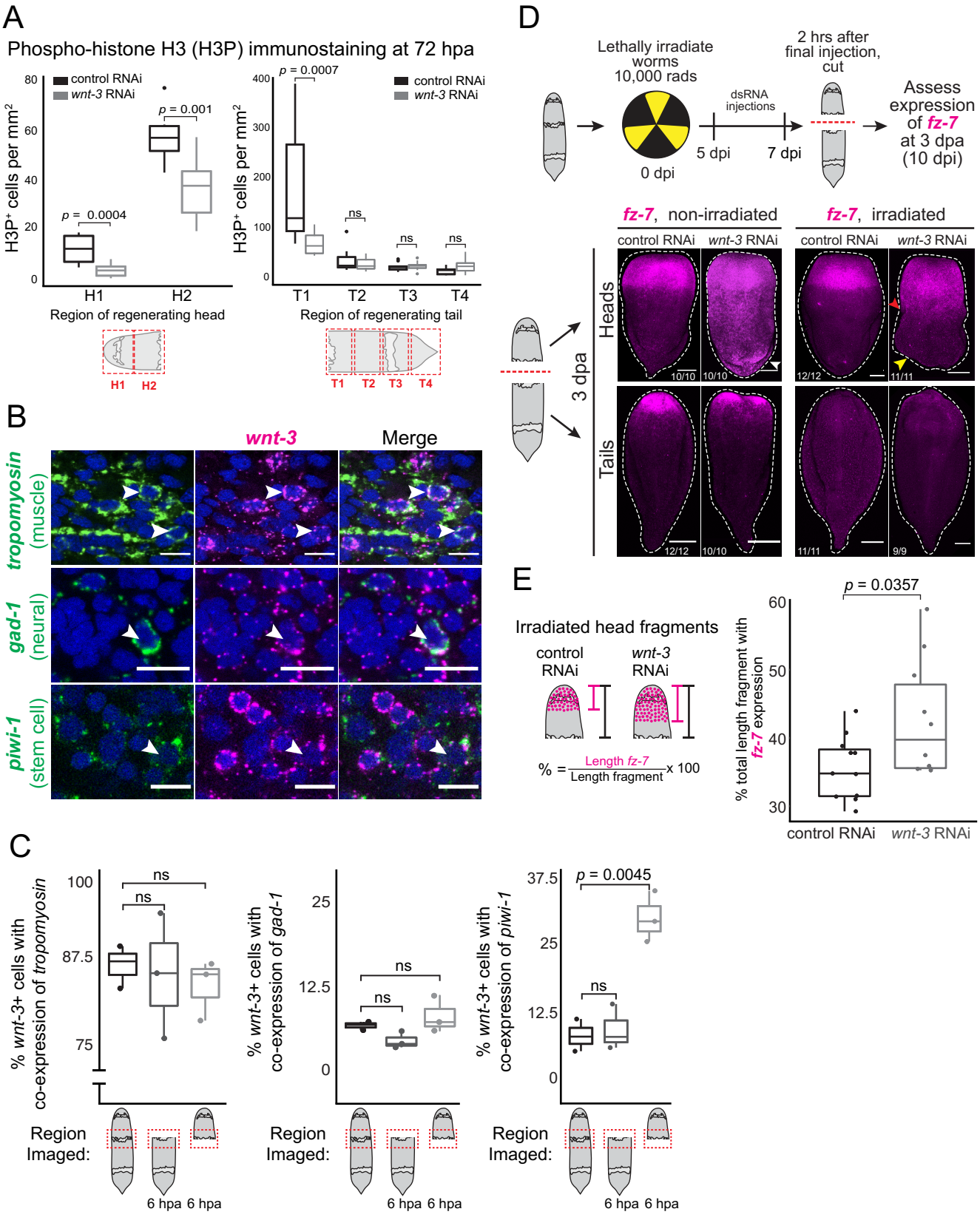
A
Phospho-histone H3 (H3P) immunostaining at 72 hpa
control RNAi
wnt-3 RNAi
H3P+ cells per mm2
p = 0.0004
p = 0.001
H1
H2
Region of regenerating head
p = 0.0007
ns
T1
T2
T3
T4
Region of regenerating tail
B
wnt-3
Merge
tropomyosin (muscle)
gad-1 (neural)
piwi-1 (stem cell)
C
% wnt-3+ cells with co-expression of tropomyosin
% wnt-3+ cells with co-expression of gad-1
% wnt-3+ cells with co-expression of piwi-1
p = 0.0045
Region Imaged:
6 hpa
D
Lethally irradiate worms 10,000 rads
0 dpi
dsRNA injections
5 dpi
7 dpi
2 hrs after final injection, cut
Assess expression of fz-7 at 3 dpa (10 dpi)
fz-7, non-irradiated
fz-7, irradiated
3 dpa
Heads
Tails
E
Irradiated head fragments
% = Length fz-7 / Length fragment x 100
p = 0.0357
% total length fragment with fz-7 expression

Figure 4

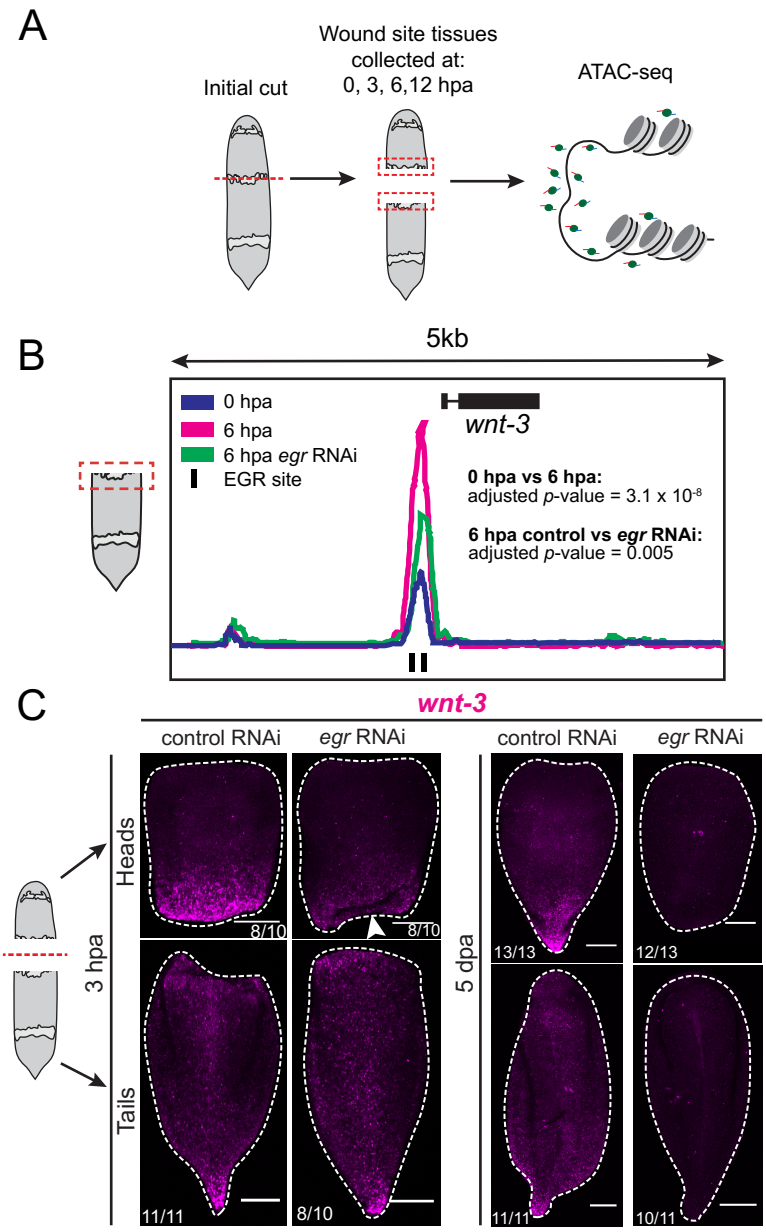
A
Initial cut
Wound site tissues collected at: 0, 3, 6,12 hpa
ATAC-seq
B
5kb
0 hpa
6 hpa
6 hpa egr RNAi
EGR site
wnt-3
0 hpa vs 6 hpa:
adjusted p-value = 3.1 x 10-8
6 hpa control vs egr RNAi:
adjusted p-value = 0.005
C
wnt-3
control RNAi
egr RNAi
control RNAi
egr RNAi
Heads
Tails
3 hpa
5 dpa
8/10
8/10
13/13
12/13
11/11
8/10
11/11
10/11

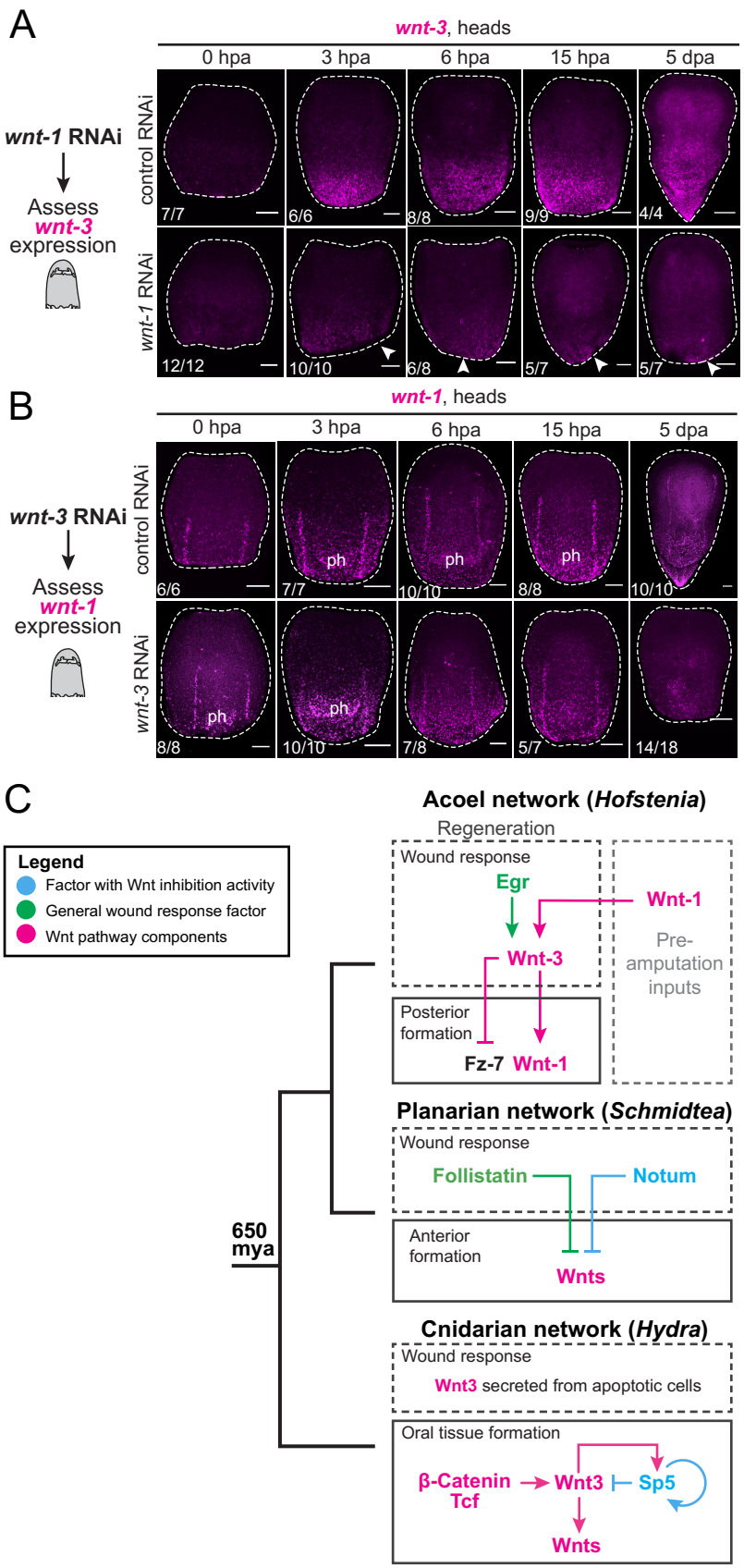
A
wnt-3, heads
0 hpa
3 hpa
6 hpa
15 hpa
5 dpa
wnt-1 RNAi
Assess wnt-3 expression
control RNAi
wnt-1 RNAi
7/7
6/6
8/8
9/9
4/4
12/12
10/10
6/8
5/7
5/7
B
wnt-1, heads
wnt-3 RNAi
Assess wnt-1 expression
control RNAi
wnt-3 RNAi
ph
6/6
7/7
10/10
8/8
10/10
8/8
10/10
7/8
5/7
14/18
C
Legend
Factor with Wnt inhibition activity
General wound response factor
Wnt pathway components
650 mya
Acoel network (Hofstenia)
Regeneration
Wound response
Egr
Wnt-1
Wnt-3
Pre-amputation inputs
Posterior formation
Fz-7
Wnt-1
Planarian network (Schmidtea)
Wound response
Follistatin
Notum
Anterior formation
Wnts
Cnidarian network (Hydra)
Wound response
Wnt3 secreted from apoptotic cells
Oral tissue formation
β-Catenin
Tcf
Wnt3
Sp5
Wnts

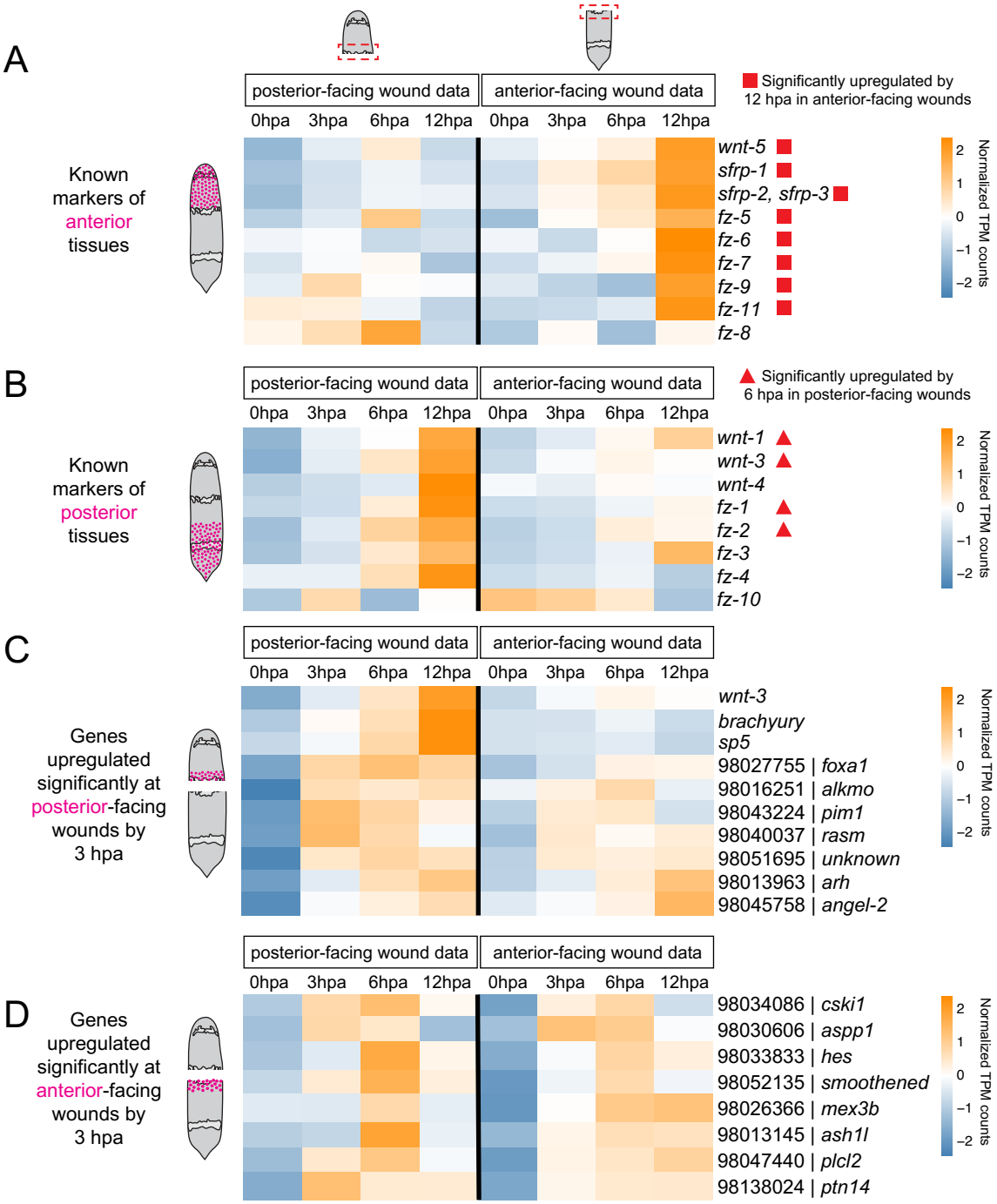

Supplemental Figure 1, Related to Figure 1: (A, B) Expression of Wnt ligands during regeneration. Expression of known markers of anterior or posterior identity was established by 6-12 hpa in anterior- or posterior-facing wound sites. Heatmap of normalized TPM (transcript per million, compared to 0 hpa) values of published markers with known anterior (A) or posterior (B) *in situ* hybridization patterns in *Hofstenia*. Gene names at right are from (Srivastava *et al.*, 2014). (C, D) Regeneration transcriptome analysis identified genes with asymmetric expression in anterior- or posterior-facing wound sites by 3 hpa. Heatmap of normalized TPM values of genes significantly upregulated by 3 hpa in anterior- (C) or posterior-facing (D) wound sites during regeneration identified in our analysis. Normalized TPM values shown from 0 hpa to 12 hpa in both fragments. Gene names depicted were the closest human BLAST hit or if previously described, published gene name was used. Datasets from (Gehrke *et al.*, 2019).

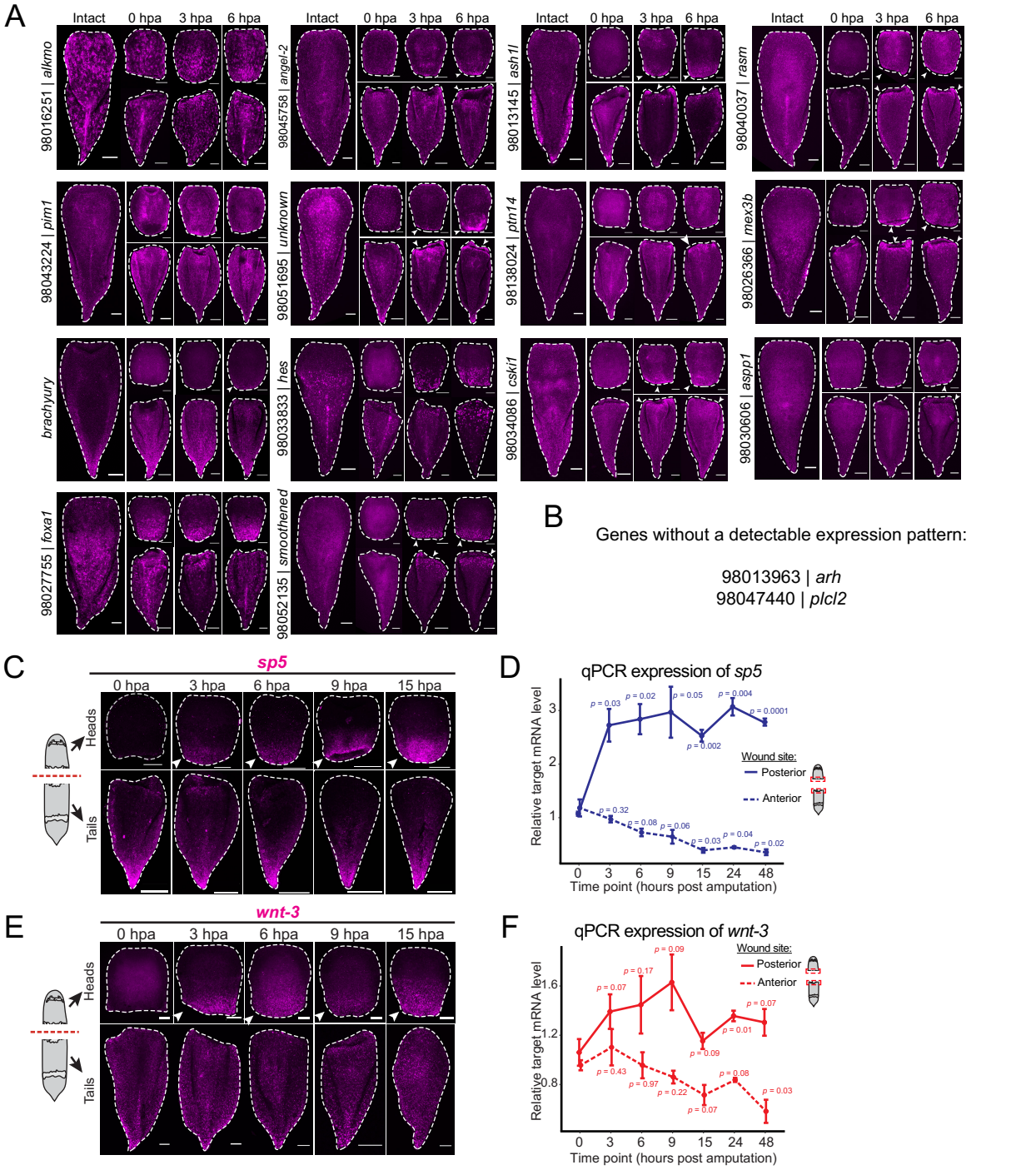

Supplemental Figure 2, Related to Figure 1: Validation of candidate genes by *in situ* hybridization of regenerating fragments. (A) *in situ* hybridization patterns for all genes we were able to obtain detectable expression patterns for at 0 hpa, 3 hpa, 6 hpa, and in intact animals (16/18). Some genes were expressed at both wound sites (*rasm*, *angel-2*, *unknown*, *smoothened*, *mex3b*, *ash1*, *cski1*, *aspp1*; white arrowheads) or if only expressed at one wound site, no earlier than 6 hpa (*brachyury*, *ptn14*; white arrowheads). In a subset of genes, it was difficult to determine if any wound-induced expression was present (*alkmo*, *pim1*, *foxa1*, *hes*). (B) List of the two genes (*arh*, *plcl2*) we were unable to obtain visible expression patterns for. (C-F) Expression of top candidates (*sp5*, *wnt-3*) during regeneration by *in situ* hybridization and qPCR. (C, D) Expression of *sp5* in regenerating head and tail fragments by *in situ* hybridization (C) and qPCR (D; *p*-values, Welch two-sample *t*-test). *sp5* was expressed in posterior-facing wound sites by 3 hpa, and maintained in this region at later stages of regeneration (arrowheads). (E, F) Expression of *wnt-3* in regenerating head and tail fragments by *in situ* hybridization (E) and qPCR (F; *p*-values, Welch two-sample *t*-test). *wnt-3* was also expressed in posterior-facing wound sites by 3 hpa during regeneration, and this expression was maintained at later stages during regeneration (arrowheads). All scale bars, 100µm.

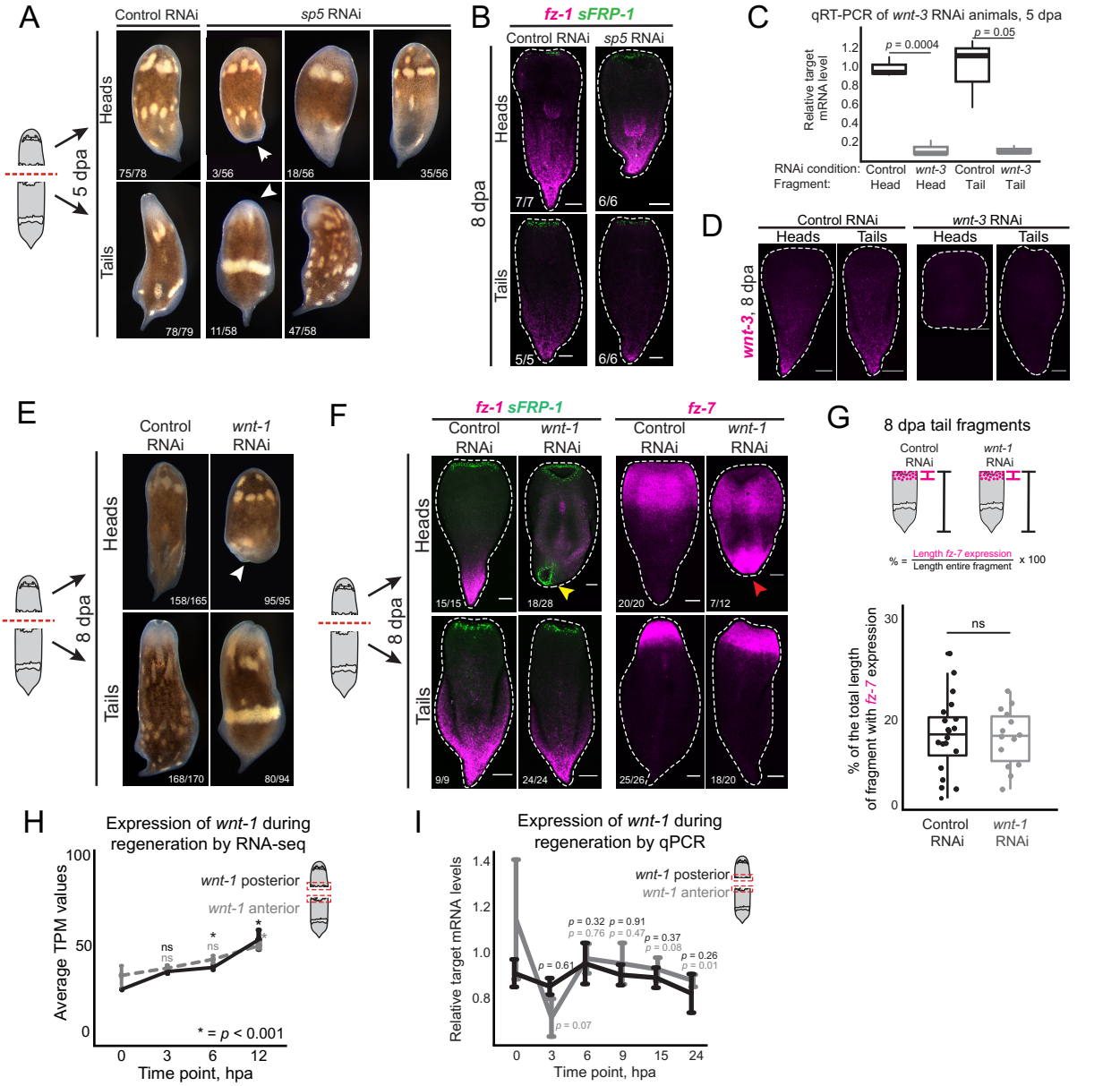

Supplemental Figure 3, Related to Figure 2: (A-B) *sp5* RNAi led to a partially penetrant regenerative phenotype. (A) Control RNAi fragments formed a new tail in head fragments (75/78) and an unpigmented blastema in tail fragments (78/79) by 5 dpa. Most *sp5* RNAi head fragments regenerated similar to control RNAi fragments (35/56, heads; 47/58, tails). Some *sp5* RNAi head fragments failed to regenerate a new tail (arrow, 3/56), or formed an outgrowth but not a fully patterned posterior (18/56). Some *sp5* RNAi tail fragments failed to form a mouth or large unpigmented blastema (7/58), or failed to regenerate completely (arrowhead, 4/58). (B) Expression of anterior and posterior markers (*fz-1*, *sFRP-1*) was unaffected following *sp5* RNAi in both head and tail fragments. (C-D) Validation of *wnt-3* RNAi by qPCR (C) and *in situ* hybridization (D) in 8 dpa RNAi fragments. Expression of *wnt-3* was lost following RNAi injections. qPCR samples are n > 3 fragments/replicate, with 3 replicates; *p*-values, Wilcoxon rank-sum test. (E-I) Characterization of *wnt-1* RNAi regenerative phenotype. (E) RNAi of *wnt-1* caused posterior regeneration defects in head fragments at 8 dpa (white arrow), compared to control RNAi head fragments. *wnt-1* RNAi tail fragments regenerated and formed a visible mouth and blastema in a similar manner to control RNAi tail fragments. (F) Expression of the anterior marker *sFRP-1* in *wnt-1* RNAi head fragments revealed new mouth formation in posterior-facing wound sites (yellow arrow), while anterior-facing wound sites expressed anterior markers in a similar manner to control RNAi. The anterior marker *fz-7* was expressed ectopically at posterior-facing wound sites following *wnt-1* RNAi (red arrow). (G) The expression domain of *fz-7* in tail fragments was the same as in control tail fragments, quantified at left (n > 13 fragments per RNAi condition; *p*-value = 0.85; Welch two-sample *t*-test; ns, not significant). (H) Expression of *wnt-1* in the RNA-seq dataset from 0 to 12 hpa. (*p*-values, likelihood ratio test; * = *p*-value < 0.001). (I) qPCR expression of *wnt-1* in anterior- and posterior-facing wounds (*p*-values, Welch two-sample *t*-test). All scale bars, 100µm.

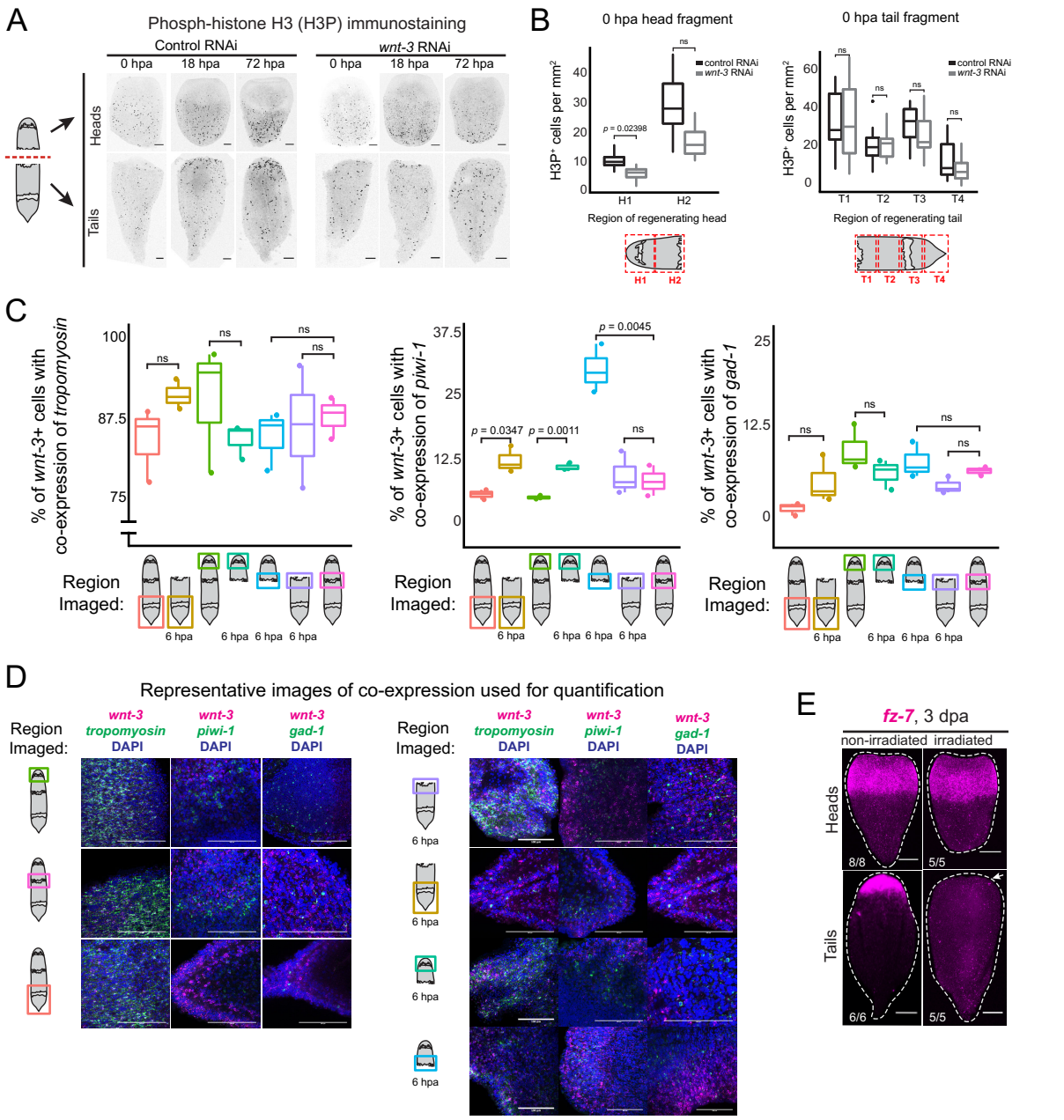

Supplemental Figure 4, Related to Figure 3: (A-B) Phospho-histone H3 (H3P) immunostaining and quantification in *wnt-3* RNAi fragments. (A) Representative images of H3P immunostaining in control and *wnt-3* RNAi regenerating fragments at 0 hpa, 18 hpa, and 72 hpa. LUT has been inverted for clarity. (B) Quantification of H3P+ foci in 0 hpa head and tail fragments following *wnt-3* or control RNAi. (n > 4 per RNAi condition/time point; *p*-value, Wilcoxon rank-sum test; ns, not significant). (C, D) Quantification of co-expression of *wnt-3* with cell type markers. (C) Co-expression was assessed in whole animals and in 6 hpa anterior- or posterior-facing wound sites, and in regions distant from the wound site in 6 hpa fragments. No significant differences were detected in numbers of *wnt-3*$^{+}$/*gad-1*$^{+}$ cells or *wnt-3*$^{+}$/*tropomyosin*$^{+}$ cells, regardless of condition or region sampled. Following amputation, co-expression of *wnt-3* and *piwi-1* was significantly increased in 6 hpa anterior- and posterior-facing wound sites compared to equivalent regions of intact animals. (*p*-values, Shapiro-Wilks Normality test, Welch two-sample *t*-test). (D) Representative samples of images used for co-expression quantification. (E) Expression of *fz-7* in wild-type and irradiated regenerating fragments. Wild-type animals expressed *fz-7* in an anterior domain in head fragments and in anterior-facing wound sites of tail fragments at 3 dpa. Tail fragments lost anterior-facing wound site expression of *fz-7* following irradiation by 3 dpa (white arrow). Numbers of fragments with shown phenotypes in the lower left corner. All scale bars, 100µm.

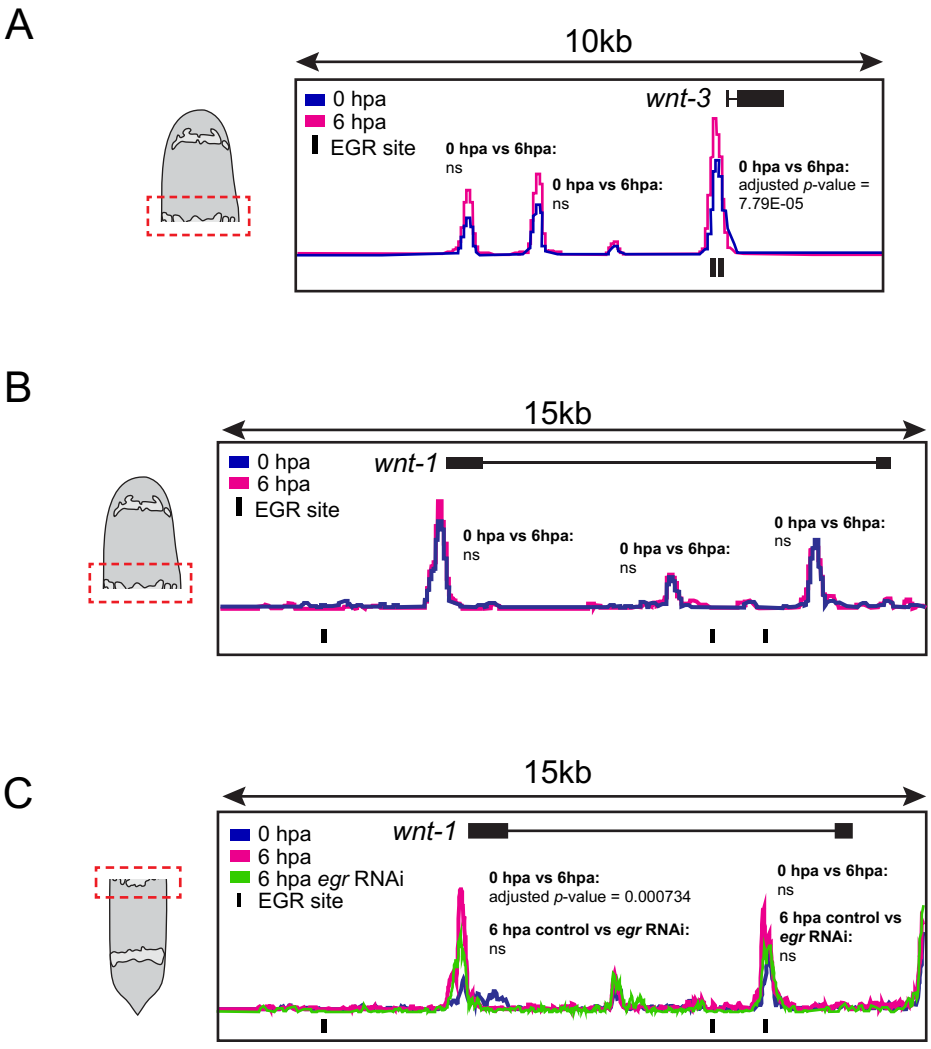

Supplemental Figure 5, Related to Figure 4: ATAC-seq data from anterior and posterior-facing wounds. (A) Schematic of the *wnt-3* genomic locus with posterior-facing wound site ATAC-seq data mapped. The promoter region contained a regeneration-responsive peak that is variable from 0 hpa (blue) to 6 hpa (magenta) (adjusted *p*-value, 7.79×10^{-5}, head dataset; Wald test). Below this accessible promoter region are two Egr binding sites. (B, C) Schematic of the *wnt-1* genomic locus with posterior-facing (B) or anterior-facing (C) wound site data mapped. (B) No significant differences in accessibility were detected at 6 hpa in the posterior-facing wound site of *wnt-1*, and Egr sites are not found within these regions. (C) Anterior-facing wound site ATAC-seq data showed a region of chromatin within the promoter of *wnt-1* that became accessible at 6 hpa (magenta) compared to 0 hpa (blue) (adjusted *p*-value, 7.34×10^{-4}, tail dataset; Wald test). Accessibility of this region was not sensitive to *egr* RNAi compared to control (green; ns, not significant; Wald test). Control RNAi track omitted for clarity. Accessibility of an additional peak (at right) within this region did not change during regeneration or in response to *egr* RNAi.

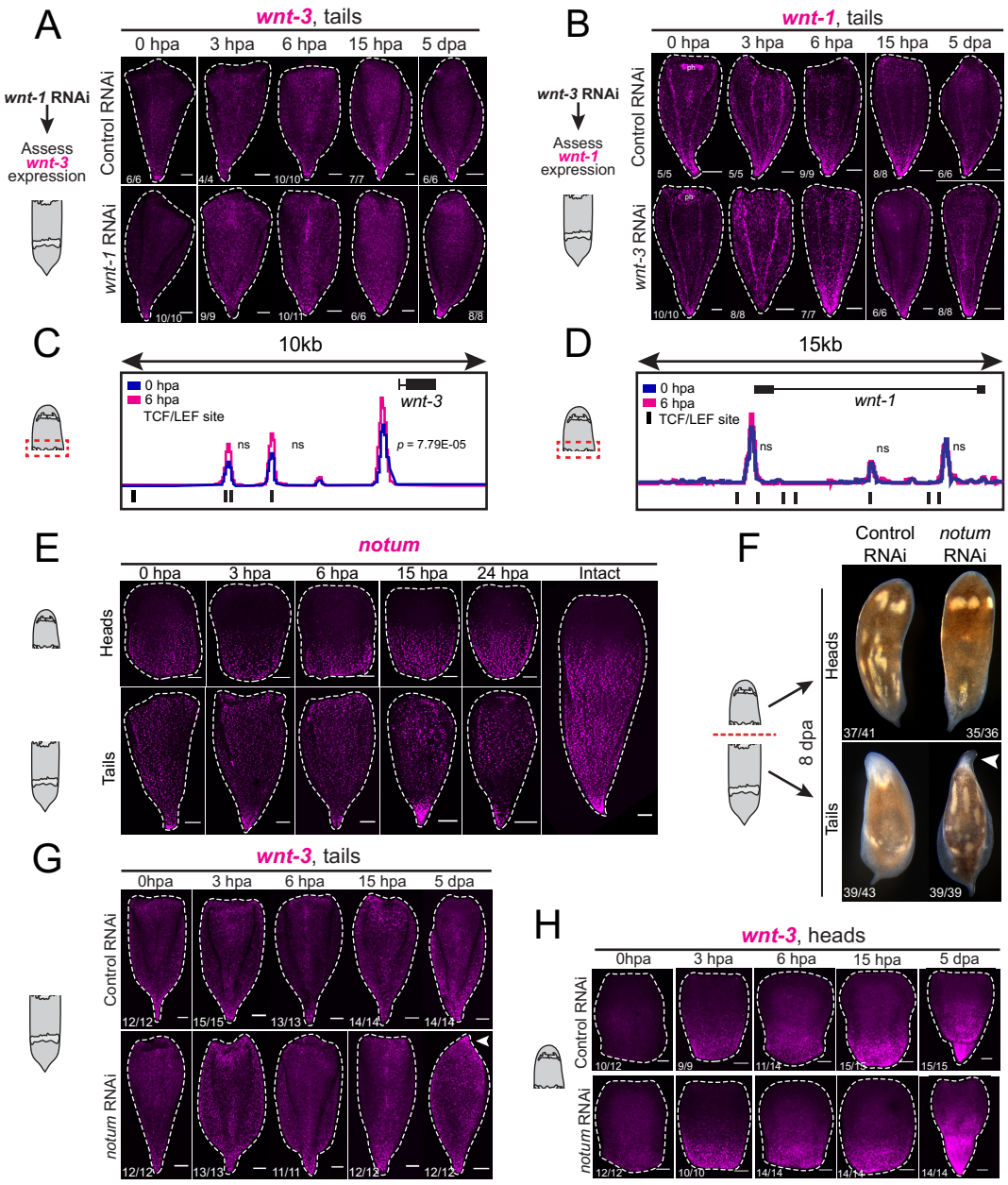

Supplemental Figure 6, Related to Figure 5: (A-D) Upregulation of *wnt-3* during regeneration relied on pre-existing expression of Wnt pathway members. (A) Expression of *wnt-3* by *in situ* hybridization in control and *wnt-1* RNAi tail fragments. The posterior gradient of *wnt-3* was maintained in both control and *wnt-1* RNAi tail fragments during regeneration. (B) Expression of *wnt-1* by *in situ* hybridization in control and *wnt-3* RNAi tail fragments. *wnt-1* was expressed in a posterior gradient in both control and *wnt-3* RNAi tail fragments during regeneration (ph, pharynx). (C) Schematic of the *wnt-3* locus with ATAC-seq data from posterior-facing wounds. There are four total TCF/LEF sites present within this region, three of which are within accessible chromatin upstream of *wnt-3*. (D) Schematic of the *wnt-1* locus with ATAC-seq data from posterior-facing wounds. There are seven total TCF/LEF sites present within this locus. Only two are within open chromatin in the promoter region. (E-H) Expression of *notum* during regeneration, RNAi phenotype, and expression of *wnt-3* during regeneration following *notum* RNAi. (E) Expression of *notum* during regeneration by *in situ* hybridization. (F) *notum* RNAi head fragments formed a posterior, but tail fragments formed an ectopic tail at anterior-facing wound sites (arrowhead; Srivastava *et al*, 2014). (G) Expression of *wnt-3* in regenerating *notum* RNAi tail fragments. Expression of *wnt-3* at early stages of regeneration was unaffected, but by 5 dpa, *wnt-3* was expressed in the ectopic posterior tissues formed at anterior-facing wound sites following *notum* RNAi (arrowhead). (H) Expression of *wnt-3* in control and *notum* RNAi head fragments. *wnt-3* was expressed in posterior-facing wound sites by 3 hpa in control and *notum* RNAi animals, and this expression was maintained at later stages during regeneration. All scale bars, 100μm.